JOURNAL OF PETROLOGY | VOLUME 43 | NUMBER 10 | PAGES 1815–1856 | 2002

Petrology and Geochemistry of the Bandas del Sur Formation, Las Cañadas Edifice, Tenerife (Canary Islands)

S. E. BRYAN[1,2]*, J. MARTÍ[3] AND M. LEOSSON[4]

[1]DEPARTMENT OF EARTH SCIENCES, MONASH UNIVERSITY, CLAYTON, VIC. 3168, AUSTRALIA

[2]CENTRE FOR MICROSCOPY AND MICROANALYSIS, UNIVERSITY OF QUEENSLAND, ST. LUCIA, QLD. 4072, AUSTRALIA

[3]INSTITUTE OF EARTH SCIENCES 'JAUME ALMERA', CSIC, LLUIS SOLE SABARIS S/N, 08028 BARCELONA, SPAIN

[4]INSTITUTE FOR PETROLOGY AND GEOCHEMISTRY, UNIVERSITÄT KARLSRUHE (TH), KAISERSTR. 12, D-76128 KARLSRUHE, GERMANY

RECEIVED NOVEMBER 10, 2001; REVISED TYPESCRIPT ACCEPTED MARCH 27, 2002

The Bandas del Sur Formation preserves a Quaternary extra-caldera record of central phonolitic explosive volcanism of the Las Cañadas volcano at Tenerife. Volcanic rocks are bimodal in composition, being predominantly phonolitic pyroclastic deposits, several eruptions of which resulted in summit caldera collapse, and alkali basaltic lavas erupted from many fissures around the flanks. For the pyroclastic deposits, there is a broad range of pumice glass compositions from phonotephrite to phonolite. The phonolite pyroclastic deposits are also characterized by a diverse, 7–8-phase phenocryst assemblage (alkali feldspar + biotite + sodian diopside + titanomagnetite + ilmenite + nosean–haüyne + titanite + apatite) with alkali feldspar dominant, in contrast to interbedded phonolite lavas that typically have lower phenocryst contents and lack hydrous phases. Petrological and geochemical data are consistent with fractional crystallization (involving the observed phenocryst assemblages) as the dominant process in the development of phonolite magmas. New stratigraphically constrained data indicate that petrological and geochemical differences exist between pyroclastic deposits of the last two explosive cycles of phonolitic volcanism. Cycle 2 (0·85–0·57 Ma) pyroclastic fall deposits commonly show a cryptic compositional zonation indicating that several eruptions tapped chemically, and probably thermally stratified magma systems. Evidence for magma mixing is most widespread in the pyroclastic deposits of Cycle 3 (0·37–0·17 Ma), which includes the presence of reversely and normally zoned phenocrysts, quenched mafic glass blebs in pumice, banded pumice, and bimodal to polymodal phenocryst compositional populations. Syn-eruptive mixing events involved mostly phonolite and tephriphonolite magmas, whereas a pre-eruptive mixing event involving basaltic magma is recorded in several banded pumice-bearing ignimbrites of Cycle 3. The periodic addition and mixing of basaltic magma ultimately may have triggered several eruptions. Recharge and underplating by basaltic magma is interpreted to have elevated sulphur contents (occurring as an exsolved gas phase) in the capping phonolitic magma reservoir. This promoted nosean–haüyne crystallization over nepheline, elevated SO_3 contents in apatite, and possibly resulted in large, climatologically important SO_2 emissions.

KEY WORDS: *Tenerife; phonolite; crystal fractionation; magma mixing; sulphur-rich explosive eruptions*

INTRODUCTION

The eruptive history of Tenerife (Canary Islands; Fig. 1) has been characterized by at least three long-term (0·2–0·5 Myr) cycles of basaltic-to-phonolitic explosive volcanism between 1·59 and 0·17 Ma (Martí *et al.*, 1994; Bryan *et al.*, 1998). These explosive cycles follow the construction of the Las Cañadas phonolitic shield volcano between >3·3 Ma and 2 Ma (Martí *et al.*, 1994). The latter eruptive history is recorded by lavas and pyroclastic deposits of the summit caldera wall [Upper Group of Martí *et al.* (1994)] and southern flanks [Bandas del Sur Formation of Bryan *et al.* (1998)] of the Las Cañadas volcano. These explosive cycles are responsible for the

*Corresponding author. Present address: Department of Earth Sciences, University of Queensland, St. Lucia, Qld. 4072, Australia. Telephone: +61 7 3365 3057. Fax: +61 7 3365 1277. E-mail: sbryan@earth.uq.edu.au

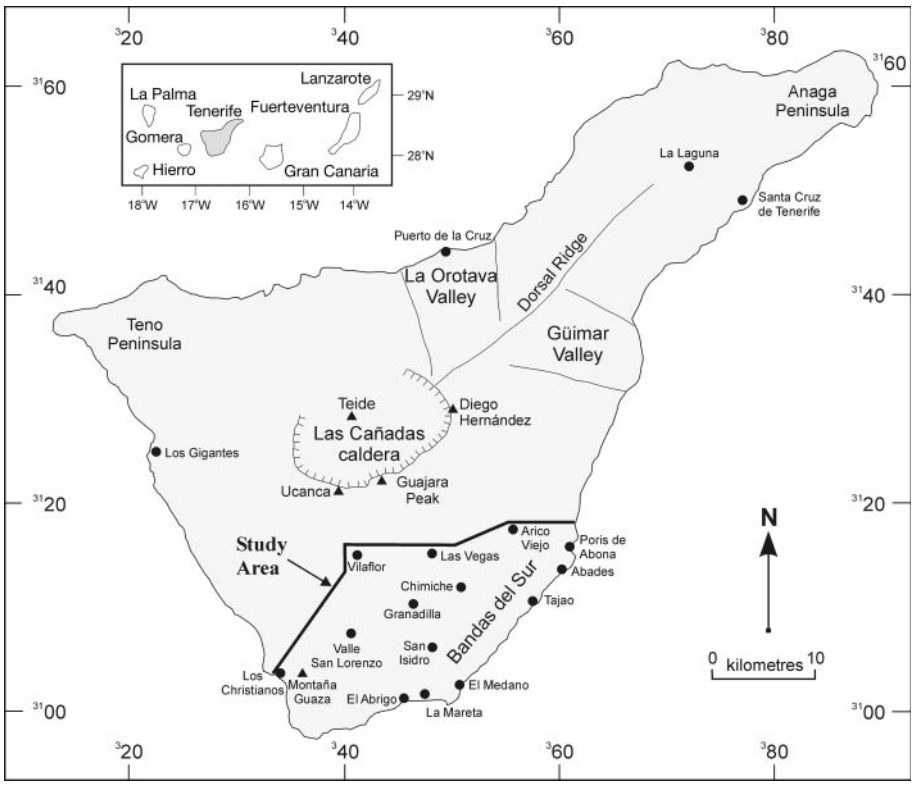

Fig. 1. Location map for Tenerife, showing the study area, principal towns mentioned in text, and geomorphological features. Inset map shows the location of Tenerife within the Canary Islands. Numbered grid represents 20 km intervals of the UTM grid (WGS84), Zone 28 for the northern hemisphere.

formation of the Las Cañadas caldera, where each ended in a major caldera-forming eruption at 1·07, 0·57 and 0·17 Ma (Martí *et al.*, 1994, 1997), although other caldera collapse events may also have occurred during these cycles. Separating the explosive cycles have been medium-term (~0·2 Myr) periods of non-explosive activity, which correspond to major erosional unconformities in the extra-caldera stratigraphy, and episodes of effusive volcanism, such as the post 0·17 Ma construction of the Teide–Pico Viejo stratovolcanic complex within the caldera (e.g. Ridley, 1970; Ablay *et al.*, 1998). Basaltic eruptions from the Dorsal Ridge, a NE-trending fissure zone extending away from the Las Cañadas caldera (Fig. 1), have been coincident with phonolitic explosive eruptions from the caldera. Ancochea *et al.* (1990) published eight ages for Dorsal Ridge basalts between 0·9 and 0·78 Ma, suggesting rapid accumulation of the thick basaltic sequences (>800 m). Phonolitic magma chambers and consequently, summit caldera development, have migrated with time to the NE, resulting in the juxtaposition of basaltic lavas sourced from the Dorsal Ridge system with proximal phonolitic pyroclastic deposits of the Las Cañadas volcano.

This paper focuses on the last two cycles of phonolitic explosive volcanism preserved in the Bandas del Sur Formation [Cycles 2 and 3 of Bryan *et al.* (1998)]. Most previous work on the geochemistry of volcanic rocks from the Bandas del Sur has not been constrained by a detailed stratigraphic framework (e.g. Fuster *et al.*, 1968; Brandle, 1973; Palacz & Wolff, 1989; Wolff & Palacz, 1989). This paper presents new mineral and whole-rock chemistry for the Bandas del Sur Formation constrained by the stratigraphy of Bryan *et al.* (1998), which provides a robust framework to interpret the petrological evolution of the Tenerife system during its most recent cycles of explosive volcanism. In detail, each of the individual eruptive units can exhibit considerable variation in mineral and/or whole-rock chemistry, as shown for the Granadilla Member (Bryan, 1998; Palacz & Wolff, 1989). A detailed examination of both the mineral and whole-rock chemistry for each eruptive unit or pyroclastic member of the Bandas del Sur Formation is therefore beyond the scope of this paper.

Figure 2 shows the stratigraphic relationship of pyroclastic and lava members of the Bandas del Sur Formation for which mineral and/or whole-rock chemical data have been obtained in this study. Most members have been defined previously, and the reader is referred to Bryan *et al.* (1998) for relevant lithological information. Some units are defined here for the first time and the

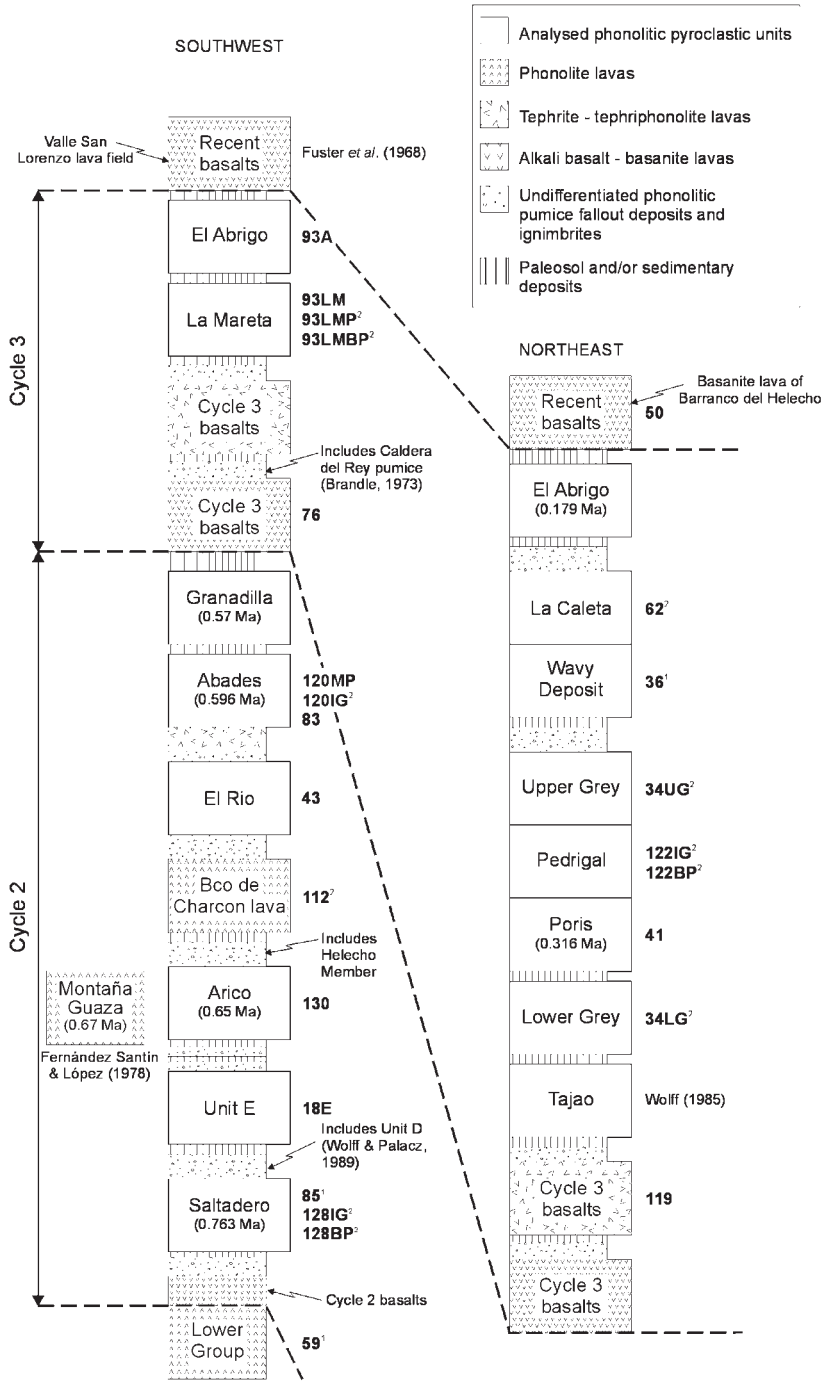

Fig. 2. Sample stratigraphy of the Bandas del Sur Formation, illustrating the stratigraphic relationships of lava and pyroclastic units described in this paper. The thickness of each unit is not to scale. Bold numbers are sample numbers referred to in figures, tables and Appendix A. [1]Whole-rock (XRF) data only; [2]electron microprobe data only. Geochemical data for other units used in this paper denoted by references.

lithological characteristics are briefly described. Electron microprobe data for minerals and pumice glass have been given by Bryan (1998) and whole-rock geochemical data are given in Appendix A. Selected whole-rock and pumice glass analyses have previously been published by Bryan *et al.* (1998). Field locations referred to in this paper by their X,Y co-ordinates and the numbered grid in figures are based on Zone 28 of the Universal

Transverse Mercator (UTM) grid for the northern hemisphere (WGS84 datum). The complete mineral, glass and whole-rock geochemical datasets can be downloaded from the *Journal of Petrology* website at http://www.petrology.oupjournals.org. Details of analytical techniques are given in Appendix B.

Previous studies

Wolff (1983) and in subsequent papers (Wolff, 1984, 1985; Wolff & Storey, 1984; Palacz & Wolff, 1989; Wolff & Palacz, 1989) has presented the only petrological studies of pyroclastic units from the Bandas del Sur Formation. Major element compositions of some eruptive units have been presented elsewhere [Montaña Guaza (Fernández Santín & López, 1978), Arico Ignimbrite Member (Schmincke & Swanson, 1967) and Caldera del Rey (Brandle, 1973; Paradas Herrero & Fernández Santín, 1984)]. Previous studies of Tenerife petrology (e.g. Ridley, 1970; Wolff & Storey, 1984; Mitjavila, 1990; Ablay *et al.*, 1995*a*, 1998; Ablay, 1997) provide compelling data for magma evolution largely by fractional crystallization. Wolff & Storey (1984) proposed that low-density phonolitic magma, generated by sidewall crystallization, accumulated at the top of the system above intermediate (tephriphonolitic) magma. Based on studies of pyroclastic units of the Bandas del Sur Formation, magma mixing (Wolff, 1985) and assimilation–fractional crystallization (AFC; Wolff & Palacz, 1989) also have been considered important in the evolution of some phonolite magmas. The role of these processes in producing geochemical variation within the Bandas del Sur Formation will be discussed below, following description of the mineral and whole-rock chemistry.

MINERAL CHEMISTRY

A summary of the phenocryst assemblages of the various rock types is given in Table 1. Features to note are: (1) the diverse phenocryst assemblage of the phonolitic pyroclastic members; (2) the generally lower phenocryst contents, restricted phenocryst assemblage and lack of hydrous phases in the phonolite lavas; (3) the presence of kaersutite as the stable hydrous ferromagnesian phase for intermediate compositions (phonotephrite to tephriphonolite), but its absence with olivine (Ablay *et al.*, 1995*b*); (4) the presence of modal feldspathoids (nosean or haüyne) in the intermediate to felsic rocks.

In the following sections, detailed descriptions of the petrography and phase chemistry are given for each of the main phonolitic pyroclastic members and interbedded basaltic to phonolitic lava units of the Bandas del Sur Formation.

Cycle 2 phonolitic pyroclastic members

Saltadero Ignimbrite Member

The Saltadero Ignimbrite is the one of the older eruptive units of the Bandas del Sur Formation for which petrological and geochemical data are available (Fig. 2). Many feldspar phenocrysts show rounding of corners, but are otherwise unresorbed. Feldspars within (banded) pumice clasts and as liberated crystal grains in the ignimbrite show some variation in composition (Fig. 3), but zoning patterns (Fig. 4) identify two anorthoclase feldspar populations ($\sim Or_{18–23}$ and $Or_{25–35}$). The high-Or anorthoclase feldspar population have low Ba contents ($\leq 0{\cdot}1$ wt % BaO) in comparison with the lower Or feldspars (up to 0·8 wt % BaO).

Clinopyroxene phenocrysts show restricted compositions in terms of Ca–Mg–Fe components and limited Na enrichment (Fig. 5). Biotite compositions are also very uniform (Fig. 6), Mg-rich ($X_{phl} = 0{\cdot}63–0{\cdot}67$) and contain moderately elevated fluorine contents ($\sim 0{\cdot}65$ wt %).

Liberated phenocrysts of titanomagnetite in the ash matrix show a narrow range in ulvöspinel solid-solution ($Usp_{33–37}$), but a spread of minor element compositions as a result of progressive MnO enrichment (Fig. 7). Titanomagnetite from pumice clasts has a slightly higher ulvöspinel content ($\sim Usp_{38}$), and is comparatively MgO-rich (2·8–3 wt %). Coexisting ilmenite contains relatively low R_2O_3 solid-solution ($ilm_{87–89}$), but two distinct populations occur, differing in MgO (Fig. 7), with the most magnesian ilmenite (up to 4·4 wt % MgO) analysed from a banded pumice clast (Fig. 7). The presence of multiple titanomagnetite and ilmenite populations (Fig. 7), and therefore discordant tie-line slopes, suggests disequilibrium. Apatite microphenocrysts and inclusions in titanomagnetite are fluorapatites [F/(F + Cl + OH) >0·5] (Fig. 8). They contain moderately high SiO_2 abundances (1·1–1·5 wt %), but relatively low SO_3 contents (<0·3 wt %; Fig. 8a), in comparison with other pyroclastic members of the Bandas del Sur Formation.

Unit E

Unit E [the notation of B. Booth & G. P. L. Walker (unpublished data collected in the 1970s)] is a plinian fallout and ignimbrite deposit described previously by Wolff & Storey (1984) and Wolff & Palacz (1989). Unit E underlies the Arico Ignimbrite Member, and two unnamed plinian-type pumice fall deposits with well-developed palaeosoils separate the two (Fig. 2). Unit E is poorly exposed within the mapped region of the Bandas del Sur, but consists of an ungraded pumice fallout deposit up to 2 m thick, which is overlain by a relatively thin (≤ 2 m thick) ignimbrite that contains occasional banded pumice and black mafic pumice. A comagmatic

Table 1: Summary of rock compositions and corresponding phenocryst assemblages for volcanic rocks of the Bandas del Sur Formation

Rock type	Phase	Assemblage
Alkali olivine basalt	Phen.	Olivine + titanian diopside + titanomagnetite (olivine > diopside)
	Gmass	Titanian diopside + titanomagnetite ± olivine ± plagioclase
Basanite	Phen.	Olivine + (titanian) diopside + titanomagnetite (olivine ≈ diopside)
	Gmass	Plagioclase + diopside ± titanomagnetite
Tephrite	Phen.	Titanomagnetite + diopside ± plagioclase
	Gmass	Plagioclase + diopside + apatite
Phonotephrite–tephriphonolite	Phen.	Plagioclase + kaersutite + diopside + titanomagnetite + apatite + haüyne ± ilmenite
	Gmass	Plagioclase + kaersutite + diopside + Fe–Ti oxides
Phonolite (lava)	Phen.	Alkali feldspar + titanomagnetite + diopside ± haüyne
	Gmass	Alkali feldspar + titanomagnetite ± diopside ± aegirine ± nepheline
Phonolite (pyroclastic)	Phen.	Alkali feldspar + biotite + sodian diopside + titanomagnetite + ilmenite + nosean/haüyne + titanite + apatite ± nepheline

Phen., phenocryst; Gmass, groundmass.

relationship with the Granadilla Member has been proposed in previous work (Wolff & Palacz, 1989). Like the Granadilla Member, the pumice fall deposit of unit E also exhibits a 'cryptic' compositional zonation of trace element abundances (Wolff & Storey, 1984). The phenocryst assemblage comprises anorthoclase (Fig. 3), diopside, biotite, titanite and Fe–Ti oxides (Wolff & Palacz, 1989). Pumice clasts from the middle of the fallout unit have been sampled and analysed in this study.

Feldspar phenocryst compositions are weakly zoned potassic anorthoclase ($Or_{31–36}$; Figs 3 and 4), containing low abundances of Ba (<0·1 wt % BaO). Diopside phenocrysts are relatively Fe- and Na-enriched, compared with other units of Cycle 2 (Fig. 5). Biotite (Fig. 6) is Fe-enriched (X_{phl} = 0·57–0·6), and F-rich (0·71–0·8 wt %), although occupancy of the X site is comparatively low (Ca + Na + K + Ba = 0·84–0·94). The lowest ulvöspinel contents ($Usp_{26–27}$) of titanomagnetite phenocrysts analysed from pyroclastic members of Cycle 2 are observed in unit E. In terms of minor element chemistry (Fig. 7), the titanomagnetites are strongly enriched in MnO (3–3·5 wt %).

Arico Ignimbrite Member

The welded Arico Ignimbrite is distinctive in containing up to four distinct juvenile clast types: (1) coarsely feldspar-phyric obsidian; (2) cream to white, crystal-poor pumice; (3) black, feldspar-phyric pumice; (4) light brown, moderately vesicular, wavy banded (fluidal-textured) to tubed pumice containing biotite + alkali feldspar + titanomagnetite + titanite + sodian diopside + nosean. The pumice types are related to three welded colour zones within the ignimbrite (Bryan *et al.*, 1998), with the last pumice type characterizing the lower and upper orange welded zones. The black, feldspar-phyric pumice is mostly restricted to the middle grey welded zone. The obsidian clasts commonly form topography-filling concentrations in the lower part of the ignimbrite (Bryan *et al.*, 1998). The ignimbrite was sampled from the middle grey welded zone, which contains both cream–white and black pumice types. Petrographic evidence for magma mixing includes banded pumice, the mixed phenocryst assemblage (Bryan *et al.*, 1998), and divergent to bimodal phenocryst compositions.

Feldspars show an extended range of compositions (Fig. 3) from sodic to potassic anorthoclase ($Or_{19–29}$). Reversely zoned crystals are characteristic (Fig. 4). Ba abundances are variable (0–0·44 wt % BaO), being highest in the sodic anorthoclase feldspars. Clinopyroxene phenocrysts are relatively magnesian, in comparison with the underlying unit E (Fig. 5). Biotite phenocrysts are F-rich (0·61–0·88 wt %) with moderately high phlogopite contents (X_{phl} = 0·61–0·63). The ignimbrite contains several compositionally distinct phases of titanomagnetite (Usp_{40}, ~Usp_{37} and Usp_{33}), which is best illustrated by minor element compositions (Fig. 7). Nosean phenocrysts are Na-rich and have comparatively high Cl contents (Fig. 9). Rare, Mg-rich olivine grains (Fo_{80}) overlap with olivine phenocryst compositions from the younger Cycle

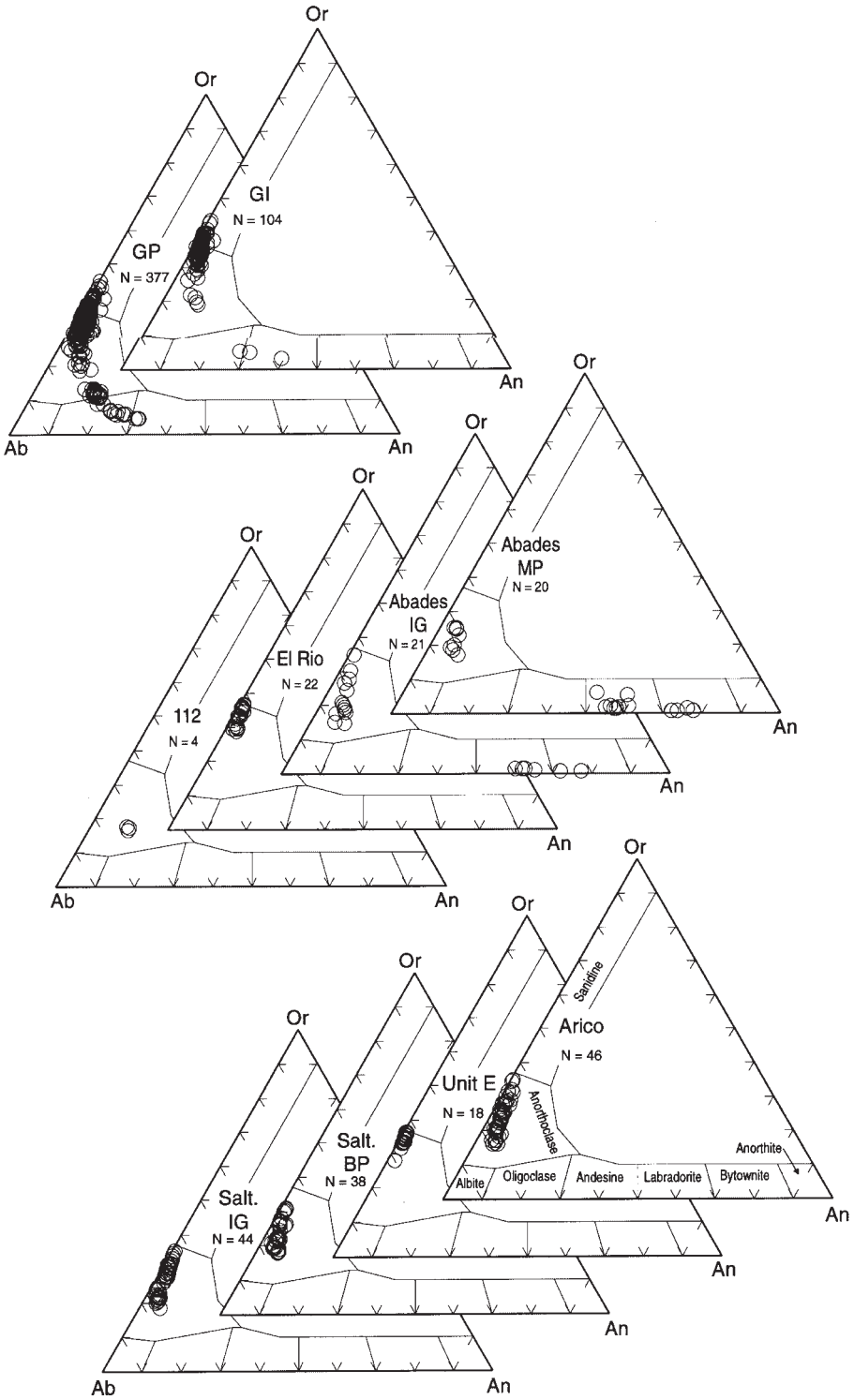

Fig. 3. Feldspar phenocryst compositions of phonolitic pyroclastic members and lavas of Cycle 2, Bandas del Sur Formation. Ab, albite; An, anorthite; Or, orthoclase; Salt., Saltadero; GP, Granadilla pumice; GI, Granadilla ignimbrite; IG, ignimbrite; BP, banded pumice; MP, mafic pumice. N, number of analyses.

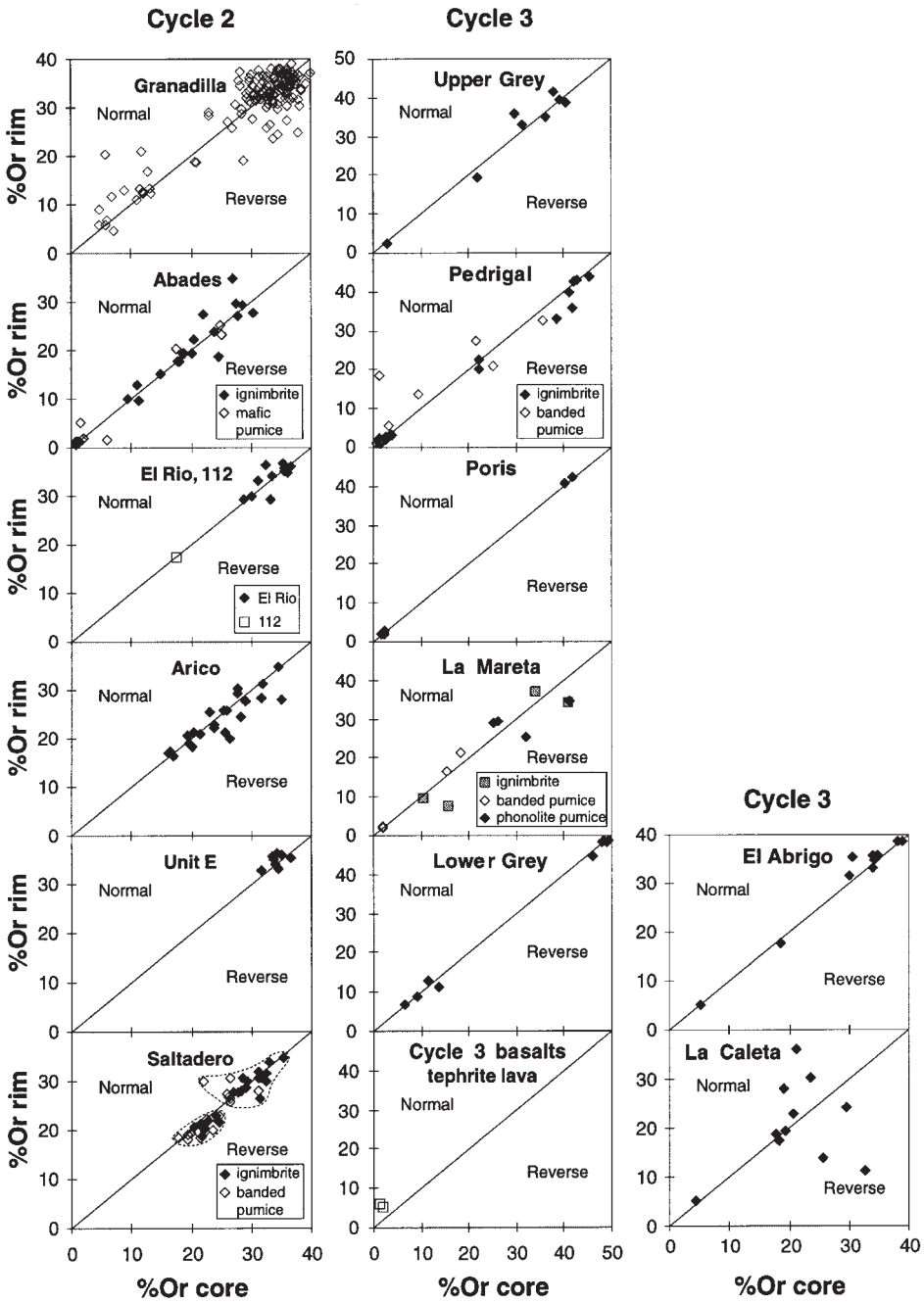

Fig. 4. Zoning patterns of feldspar phenocrysts, based on orthoclase (Or) content (molecular per cent). Core and rim analyses from the same phenocryst are plotted to illustrate the growth history of individual phenocrysts. Feldspar phenocrysts will tend towards higher orthoclase contents during fractional crystallization of magma under closed-system conditions, resulting in normal compositional zoning. Reverse compositional zoning indicates disturbance of the system (e.g. introduction of mafic magma).

3 and Recent basalt lavas (Fig. 10), and suggest a basaltic magmatic component to the Arico Ignimbrite.

El Rio Member

A pumice fall deposit ~2·5 m thick that is gradational into an overlying, distinctive, grey and white, cross-stratified to wavy stratified base surge deposit is named here the El Rio Member. The member is exposed locally along the lower reaches of the barrancos del Rio [grid reference: $^{3}53^{310}$, $^{31}10^{260}$ (barranco is a Spanish term for a steep-sided gully or valley)] and Helecho ($^{3}54^{250}$, $^{31}08^{490}$), where it directly overlies the Helecho Member

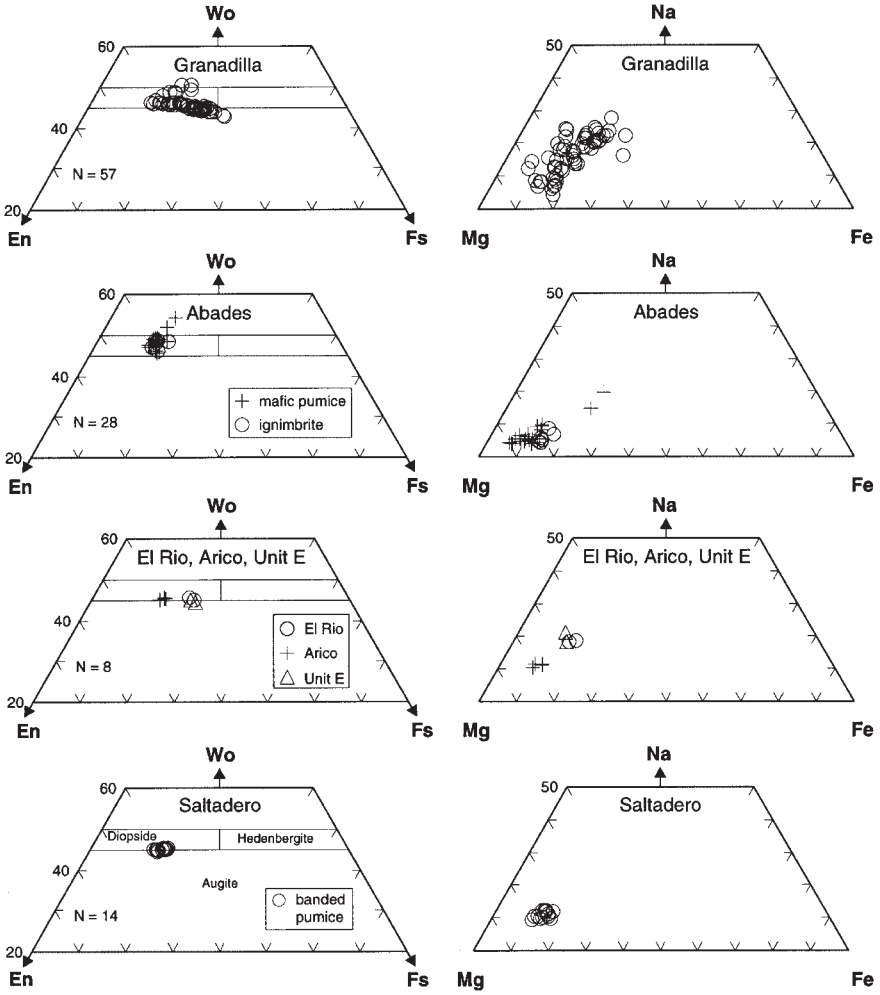

Fig. 5. Clinopyroxene phenocryst compositions of Cycle 2 phonolitic pyroclastic units, expressed in terms of the three-component system wollastonite (Wo)–enstatite (En)–ferrosilite (Fs); and Mg–Fe–Na (atomic per cent) relationships. Field boundaries after Morimoto (1988). N, number of analyses.

and underlies the Abades Ignimbrite Member (Fig. 2; Bryan, 1998). The member is of interest because it is the last plinian fall deposit of Cycle 2 before the culminating eruption of the Granadilla Member. Pumice clasts from the fall unit have been analysed in this study.

Phenocryst compositions show a close similarity to those of unit E, suggesting that these plinian fall deposits record eruptions from similarly evolved phonolite magmas. Feldspars are potassic anorthoclase ($Or_{31–37}$; Fig. 3), and low in Ba (<0·1 wt % BaO). Clinopyroxene phenocrysts are some of the most Fe- and Na-enriched compositions analysed from the phonolitic pyroclastic members below the Granadilla Member (Fig. 5). Biotite phenocrysts have comparatively low phlogopite (X_{phl} = 0·58), but high F (0·7–0·85 wt %) contents. TiO_2 abundances (4·4–4·7 wt %) in biotite are the lowest for the pre-Granadilla phonolitic pyroclastic members. Titanomagnetite microphenocrysts are characterized by low ulvöspinel contents ($\sim Usp_{27}$), and strong MnO enrichment (Fig. 7).

Abades Ignimbrite Member

The Abades Ignimbrite immediately underlies the Granadilla Member (Fig. 1) and therefore may be important in assessing comagmatic relationships (see Wolff & Palacz, 1989). Large mafic pumice clasts are characteristic, and in detail, are composed of a mixture of two to three magma types. Light green phonolitic glass blebs containing biotite and alkali feldspar occur sporadically within a dominant, dark brown, moderately vesicular mafic pumice glass. In addition, two types of mafic glass can be identified. A dark brown, crystal-rich glass contains phenocrysts of plagioclase, kaersutite, titanomagnetite, and megacrysts of titanian diopside. A subordinate light

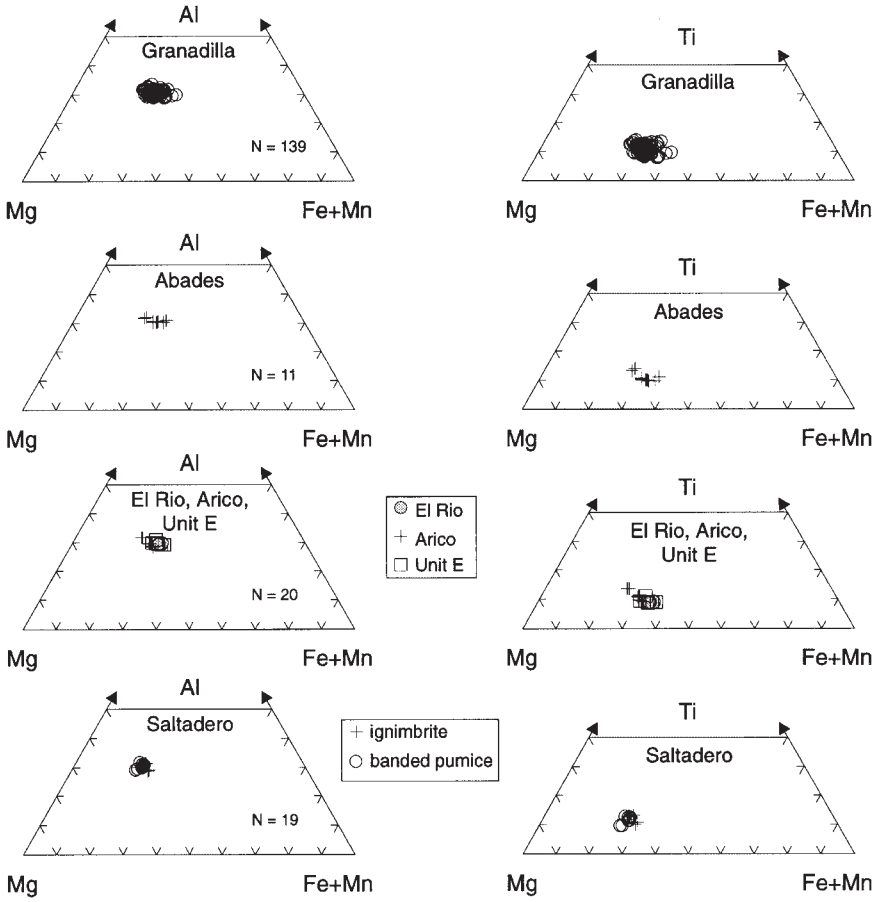

Fig. 6. Biotite phenocryst compositions (atomic per cent), Cycle 2, Bandas del Sur Formation. N, number of analyses.

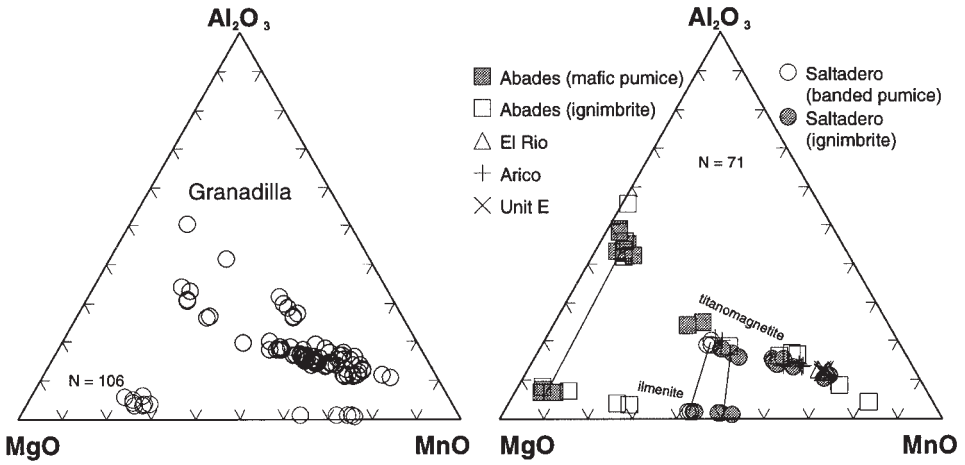

Fig. 7. Minor element compositions of coexisting titanomagnetite and ilmenite, Cycle 2, Bandas del Sur Formation. Tie-lines join coexisting minerals interpreted to be in equilibrium. N, number of analyses.

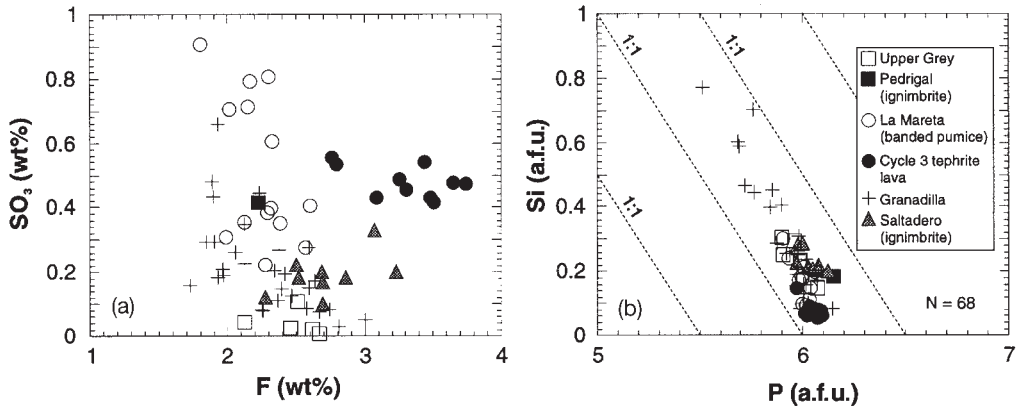

Fig. 8. (a) SO_3 vs F and (b) Si vs P (O = 26) relationships of apatite microphenocrysts and inclusions. N, number of analyses; a.f.u., atoms per formula unit.

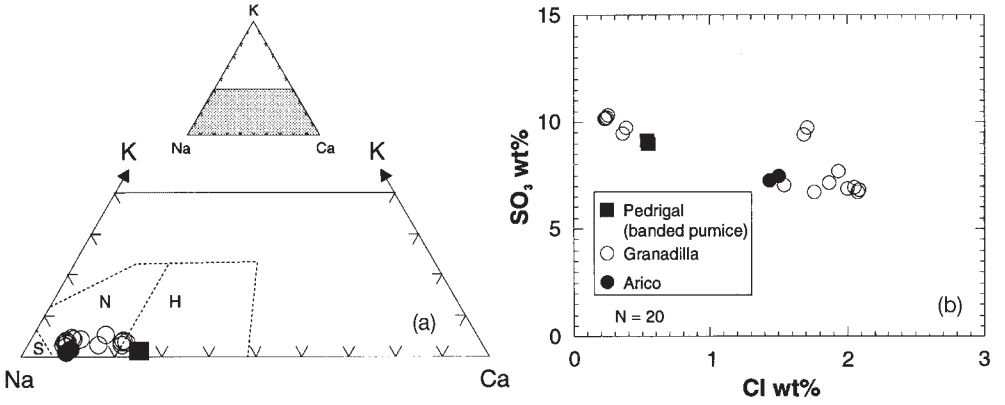

Fig. 9. Nosean–haüyne phenocryst compositions, expressed in terms of (a) Na, K and Ca (atomic per cent) and (b) SO_3 vs Cl contents. Field boundaries in (a) after Lessing & Grout (1971). S, sodalite; N, nosean; H, haüyne. N, number of analyses.

brown glass lacks the large kaersutite and diopside phenocrysts, but contains microphenocrysts of kaersutite, diopside and plagioclase, and microlites of kaersutite. Apatite occurs as inclusions in both kaersutite and titanomagnetite.

Three to four feldspar populations are identified (Figs 3 and 4): bytownite ($Ab_{25}An_{74}Or_1$), labradorite ($Ab_{40}An_{58}Or_2$), calcic anorthoclase ($Ab_{76}An_9Or_{15}$–$Ab_{74}An_6Or_{23}$) and potassic anorthoclase ($Ab_{71}An_4Or_{25}$–$Ab_{64}An_1Or_{35}$). Feldspar phenocrysts exhibit both reverse and normal zoning patterns (Fig. 4), although many are homogeneous. The highest Ba abundances (up to 0·9 wt % BaO) occur in the calcic anorthoclase feldspars.

Diopside phenocrysts are relatively magnesian (Fig. 5) and Ti-rich (0·8–3·1 wt % TiO_2). Two populations can be distinguished, based on Ti content ($\geq$2 wt % and <1·2 wt % TiO_2) and Na enrichment (Fig. 5), and correspond to the pale brown and pale green diopsides observed in thin section. Some liberated diopside grains in the matrix of the ignimbrite have overgrowths of kaersutite. Magnesian kaersutite phenocrysts show little compositional variation (Fig. 11) and have low fluorine contents. Biotite exhibits a range in phlogopite (X_{phl} = 0·63–0·55) and TiO_2 (5–7·3 wt %) content, and elevated F abundances (0·5–0·8 wt %), but compositions are within the range of those observed for other Cycle 2 ignimbrites. Several compositionally distinct populations of Fe–Ti oxides are present (Fig. 7), including four different spinel compositions, distinguished by ulvöspinel contents (Usp_{30}, Usp_{38}, $Usp_{42–45}$ and Usp_{64}), and minor element chemistry (Fig. 7). Cr-bearing titanomagnetite (containing >0·5 wt % Cr_2O_3) is also present. The most Mg-rich ilmenite population provides a consistent tie-line slope with the most Mg-rich titanomagnetite (Fig. 7). R_2O_3 solid-solution in the ilmenites is between 13 and 15%. Rare grains of olivine in the ignimbrite are Mg-rich ($\sim Fo_{80}$), and have moderately high levels of Ca

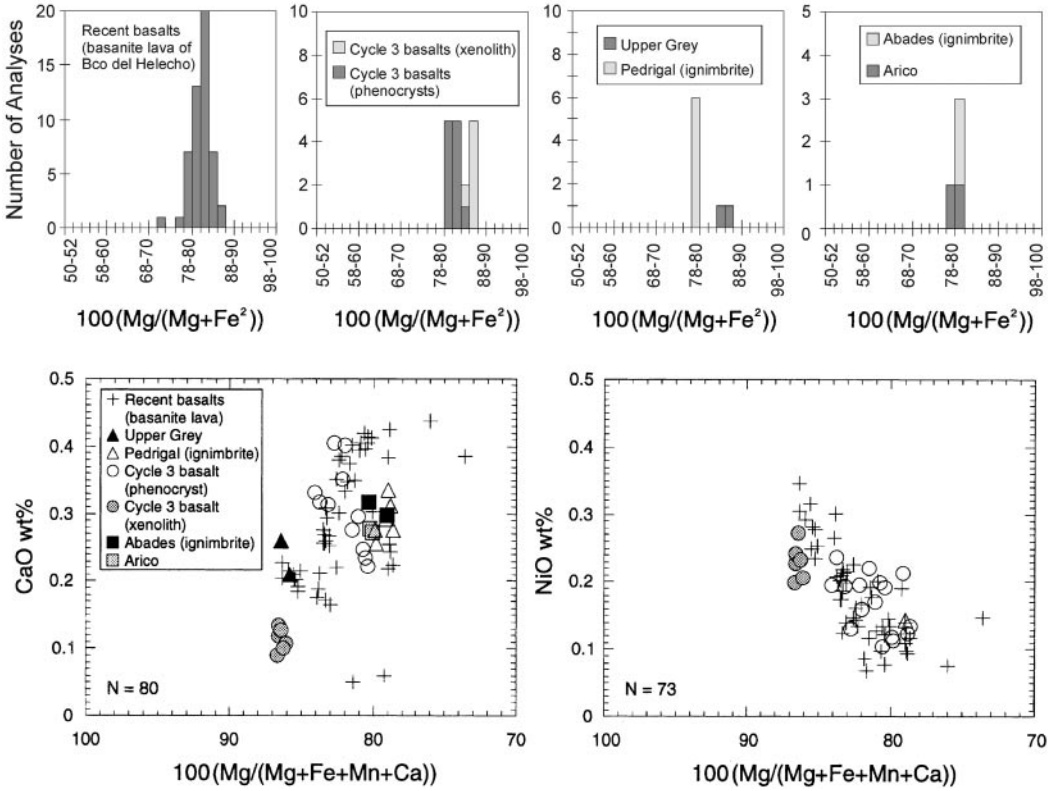

Fig. 10. Histograms of olivine phenocryst compositions (atomic per cent) of basaltic lavas and olivine grain compositions in the phonolitic ignimbrites of the Bandas del Sur Formation. Also shown are CaO and NiO contents in olivine vs olivine composition (atomic per cent). Bco, barranco; N, number of analyses.

solid-solution (Fig. 10). Cr-bearing titanomagnetite and olivine are diagnostic of the basaltic lavas (see below).

Granadilla Member

The Granadilla Member has the been the focus of several studies (e.g. Wolff & Storey, 1984; Palacz & Wolff, 1989; Wolff & Palacz, 1989), which have largely dealt with whole-rock data, and only one titanite analysis has been published (Wolff, 1984). The member is one of the most widely dispersed and largest volume pyroclastic units at Tenerife, and represents the culminating eruption to a penultimate cycle of explosive volcanism of the Las Cañadas volcano (Bryan *et al.*, 1998, 2001). The eruptive stratigraphy comprises three plinian pumice fall units (units 1, 3 and 4) and an intervening thin phreatoplinian ash bed (unit 2), with unit 4 overlain by the widespread Granadilla ignimbrite (unit 5). The mineral chemistry has been discussed in detail by Bryan (1998), and is summarized here. Pumices contain the phenocryst assemblage alkali feldspar, biotite, sphene, nosean–haüyne, sodian diopside, titanomagnetite, ilmenite, and apatite. Alkali feldspar is the dominant phenocryst phase in all units. Kaersutite and plagioclase are subordinate phenocryst phases in pumices from units 1 and 3, and in the upper parts of the Granadilla ignimbrite (unit 5). Kaersutite also occurs as liberated crystal grains in units 2 and 5. Blebs of crystal-rich, poorly vesicular glass are relatively common in pumices from unit 1 and contain fine-grained (poikilitic) intergrowths of plagioclase, kaersutite, Fe–Ti oxides $\pm$ apatite.

Feldspar compositions show a relatively restricted range from potassic anorthoclase to sodic sanidine ($Or_{30–40}$; Fig. 3). In some pumice clasts, however, two to three feldspar populations occur with the presence of calcic anorthoclase to andesine phenocrysts, and the plagioclase phenocrysts are resorbed. Generally strong zoning patterns are observed for feldspar phenocrysts (Fig. 4), and both normally and reverse zoned populations occur. The calcic anorthoclase phenocrysts contain the highest BaO contents (up to 2 wt %). Light green euhedral clinopyroxene often forms glomerocrysts with titanomagnetite and defines a continuous series from diopside to aegirine augite compositions ($En_{39}Fs_{15}Wo_{46}$–$En_{27}Fs_{30}Wo_{43}$). Pyroxenes are predominantly unzoned, although a strongly reverse zoned phenocryst population is evident in the Granadilla ignimbrite (unit 5). Biotite is the dominant hydrous phase and is Mg-rich [Mg/(Mg + Fe) $\sim$0·6–0·55], Cl-poor, and with generally elevated fluorine contents (0·6–

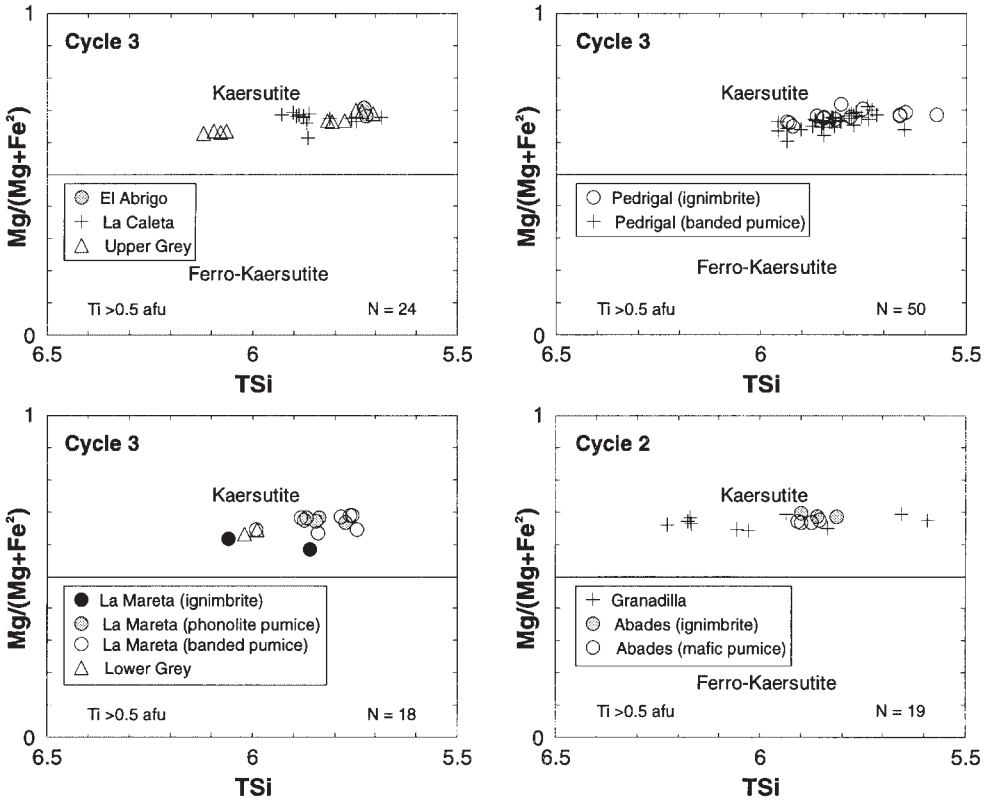

Fig. 11. Phenocryst kaersutite compositions of phonolitic pyroclastic members of the Bandas del Sur Formation. Cation proportions are based on the 13–(Ca + Na + K) normalization procedure (Robinson *et al.*, 1981), and the prefix T denotes cation in the tetrahedral site. N, number of analyses.

0·9 wt % F). Ulvöspinel solid-solution of titanomagnetite phenocrysts is in the range of $Usp_{27–43}$ whereas ilmenite shows a more restricted compositional range ($Ilm_{88–93}$). Several compositionally distinct Fe–Ti oxide populations have been identified within individual pumice clasts. Fluorapatites [F/(F + Cl + OH) >0·5], typically occurring as inclusions within titanomagnetite and biotite phenocrysts, contain high SiO_2 (up to 3·5 wt %), SO_3 ($\leq$0·7 wt %; Fig. 8a) and light rare earth element (LREE) contents (up to 8 wt %) with Ce_2O_3 predominant over La_2O_3. Feldspathoid microphenocrysts show a range of Ca content ($\leq$8 wt % CaO) that defines a gradation in composition from sodalite to haüyne, although most classify as nosean (Fig. 9). They are distinguished from true sodalite by their high sulphur contents (up to 11 wt % SO_3). Distinctive titanite phenocrysts show variable but high Zr contents (up to 2·4 wt % ZrO_2), $\sim$1 wt % Nb_2O_5, and moderate LREE (La, Ce) abundances (0·5–1 wt %).

Cycle 3 phonolitic pyroclastic members

Tajao ignimbrite

The petrology of the Tajao ignimbrite has been described by Wolff (1985). The Tajao ignimbrite is exposed only locally in outcrops along the autopista ($^{3}55^{380}$, $^{31}09^{670}$) to the west of Tajao (Fig. 1). The Tajao ignimbrite occurs near the base of Cycle 3, but its exact stratigraphic position remains uncertain. The ignimbrite overlies a well-developed palaeosol and erosional surface developed on top of the Granadilla Member. It is in turn overlain by epiclastic deposits and the Poris Member. The ignimbrite, <2 m thick, contains moderately abundant banded pumice, but two dominant pumice types can be identified: (1) a light grey to green, crystal-poor, highly vesicular pumice containing microphenocrysts of feldspar and titanomagnetite $\pm$ large phenocrysts of alkali feldspar; (2) brown, poorly to moderately vesicular, wavy to tubed pumice with large phenocrysts of plagioclase, kaersutite, titanian diopside and titanomagnetite. Apatite occurs as inclusions in the titanian diopside, whereas the large plagioclase phenocrysts are commonly resorbed or skeletal.

The ignimbrite contains a diverse phenocryst assemblage of: titanian diopside, sodian diopside, diopside, olivine, bytownite–labradorite, oligoclase–andesine, sodic sanidine, biotite, kaersutite, titanomagnetite (three compositionally distinct phases), ilmenite (two compositionally distinct phases), titanite, apatite, nepheline, nosean–

haüyne, and pyrrhotite (Wolff, 1985). The titanian diopside occurs as: (1) polymineralic aggregates with feldspar and titanomagnetite; (2) large, euhedral phenocrysts; (3) overgrowths to pale green, sodian diopside cores; (4) anhedral cores, rimmed by pale green sodian diopside. Mineral chemistry data have been published by Wolff (1985), who grouped the phenocryst phases into assemblages related to glass and whole-pumice composition. Petrographic relations, and mineral and glass chemistry were interpreted to reflect a two-stage process involving the mingling and mixing of basaltic, phonolitic and tephriphonolitic (trachyandesitic) magmas.

Lower Grey Member

The Lower Grey Member is a widespread eruptive unit comprising plinian fall deposits, accretionary lapilli tuff and an intraplinian ignimbrite (Bryan *et al.*, 1998). It occurs toward the base of Cycle 3 (Fig. 2) and is exposed extensively in the east of the Bandas del Sur, and along the northern and southern flanks of the Dorsal Ridge. The intraplinian ignimbrite has been analysed in this study.

Two compositionally distinct feldspars are present within the Lower Grey ignimbrite (Fig. 12): sodic sanidine ($Ab_{51}An_1Or_{48}$) and calcic anorthoclase–sodic andesine ($Ab_{66}An_{20}Or_{14}$–$Ab_{63}An_{30}Or_7$). The plagioclase feldspars are characteristically resorbed, but are only moderately enriched in Ba (<0·4 wt % BaO). As with feldspars, two clinopyroxene populations are present, a pale green sodian diopside with 2–2·5 wt % Na_2O (Fig. 13), and a pale brown titanian diopside with 2·7–3 wt % TiO_2. The diopside phenocrysts exhibit only weak reverse zoning patterns, although some sodian diopsides are observed in thin section to be rimmed by Fe–Ti oxides. Biotite phenocrysts have the lowest phlogopite content of the Cycle 3 pyroclastic members ($X_{phl} = 0{\cdot}52$), and relatively low abundances of TiO_2 (Fig. 14) and fluorine. Kaersutite phenocrysts show little compositional zonation (Fig. 11), and are typically low in F and Cl. Two compositionally distinct phases of titanomagnetite are distinguished by minor element abundances (Fig. 15), with an Al_2O_3- and MgO-rich (∼8 wt %) spinel prominent. Rare, anhedral grains of nepheline are also present. Wolff (1983, 1985) suggested that nepheline occurs as a phenocryst only in the most strongly fractionated phonolites on Tenerife. Another explanation for this occurrence, however, is that nepheline, instead of nosean or haüyne, may have precipitated in the absence of a sulphur- and/or chlorine-rich gas phase (Bryan, 1998).

La Mareta Ignimbrite Member

The upper parts of the La Mareta Ignimbrite contain abundant, large (≤40 cm diameter) banded pumice. Although banded pumice textures suggest the mingling of two different magma compositions, the mineral chemistry reveals a more complex history. At least four different feldspar compositions are identified (Fig. 12), three of which occur within one banded pumice clast. A sodic bytownite ($Ab_{44}An_{54}Or_2$) population is restricted to the mafic (brown) glass of banded pumice clasts. Sodic andesine to calcic oligoclase ($Ab_{68}An_{16}Or_{16}$–$Ab_{60}An_{35}An_5$) occurs as phenocrysts within the mafic and phonolitic (pale green) glass of pumice clasts, and as liberated crystal grains within the ignimbrite. Disequilibrium textures characterize this phenocryst population. A calcic anorthoclase phenocryst population within phonolitic pumice glass also exhibits resorption textures. Sodic sanidine–potassic anorthoclase ($Ab_{57}An_2Or_{41}$–$Ab_{65}An_9Or_{26}$) feldspars occur in phonolite pumice clasts and as crystal grains within the ignimbrite matrix. Some potassic anorthoclase phenocrysts in pumice clasts have rounded corners and minor embayment, but do not exhibit the strongly resorbed morphology of the plagioclase phenocrysts. High Ba contents (up to 1·5 wt % BaO) characterize the anorthoclase feldspar population. Excluding bytownite phenocrysts, feldspars are both normally and reversely zoned (Fig. 4).

There are at least two distinct compositional populations of diopside (Fig. 13): a minor sodian diopside population (>Ae_{10}), restricted to crystal grains in the ignimbrite matrix, and a dominant, Ti- and Al-rich diopside. Both diopside populations are normally and reversely zoned. Biotites form euhedral, homogeneous grains with intermediate phlogopite contents ($X_{phl} \sim 0{\cdot}55$) and Mg/(Mg + Fe) ratio (0·63). Biotite phenocrysts set in the brown (mafic) glass of banded pumice are higher in Ti (∼7·5 wt % TiO_2; Fig. 14) and Ba (∼2–3 wt % BaO), but lower in fluorine (0·25–0·35 wt % F). Kaersutite phenocrysts (Fig. 11) are homogeneous, although phenocrysts within phonolite pumice tend to have higher fluorine contents (0·1–0·2 wt %).

Coexisting Fe–Ti oxide microphenocrysts in phonolite and banded pumice clasts show diverse minor element compositions (Fig. 15). Titanomagnetite occurring as inclusions within kaersutite (in banded pumice) has high ulvöspinel (Usp_{39}) and relatively high Al_2O_3 (∼3 wt %) contents. Mn-rich titanomagnetite microphenocrysts occur within phonolite pumice and as liberated crystal grains in the ignimbrite matrix (Fig. 15). The lower Mg abundances of some titanomagnetites are interpreted to reflect some subsolidus equilibration (Fig. 15). Ilmenites are moderately enriched in MgO (∼4 wt %).

Apatite occurs as inclusions within titanomagnetite and diopside, and as microphenocrysts set in green (phonolitic) and brown (mafic) glass of banded pumice clasts. Apatites set in mafic glass (either as microphenocrysts or inclusions) are distinguished from those in phonolitic glass by their

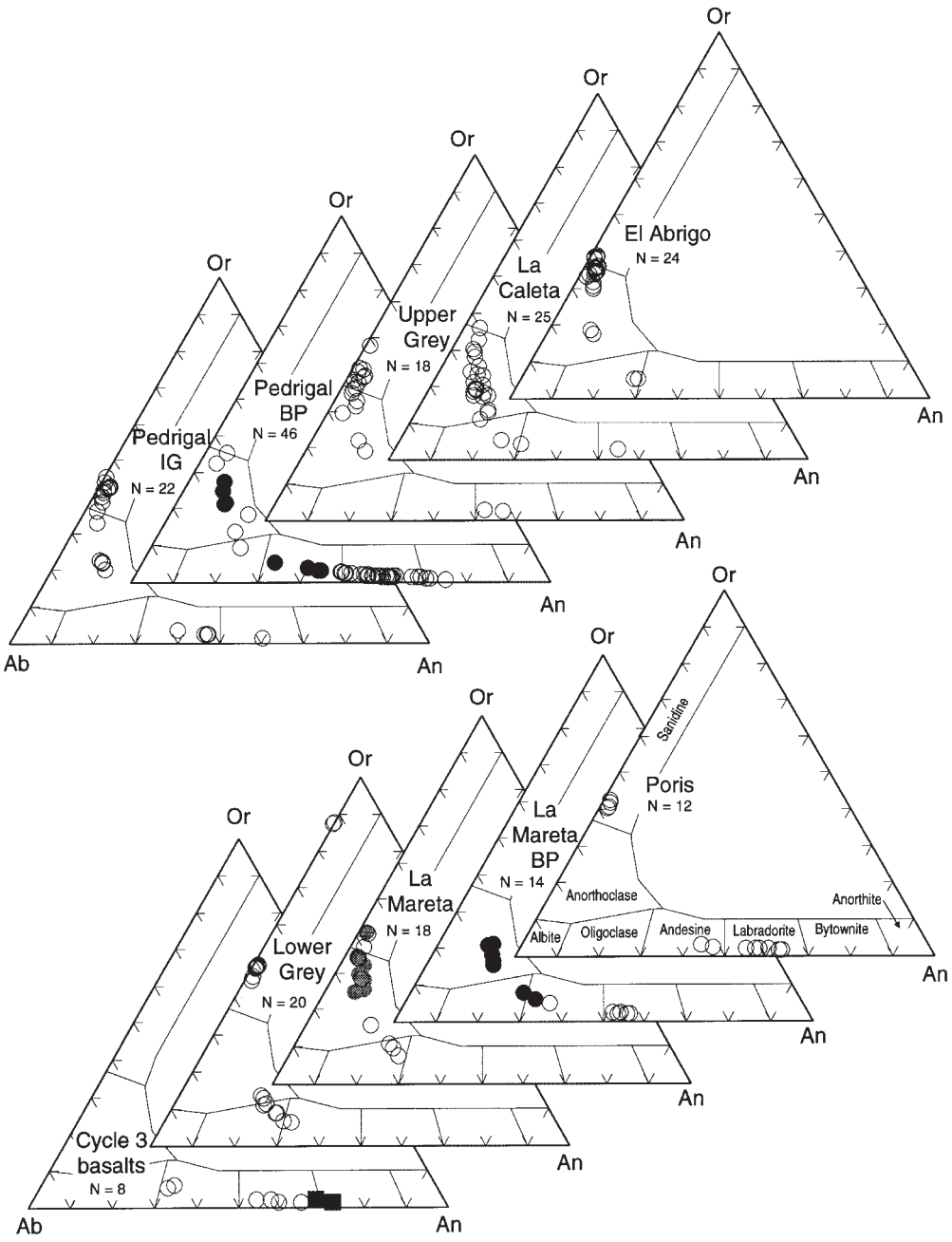

Fig. 12. Albite (Ab)–anorthite (An)–orthoclase (Or) plots of feldspar phenocryst compositions of pyroclastic units and lavas, Cycle 3, Bandas del Sur Formation. For the Cycle 3 basalts: ■, groundmass plagioclase in basalt lava (sample 76); ○, phenocryst and groundmass plagioclase in tephrite lava (sample 119). For the La Mareta Ignimbrite: grey circles, liberated feldspar grains in the ignimbrite matrix; ○, phenocrysts in pumice clasts. For the banded pumice (BP) clasts from the La Mareta and Pedrigal ignimbrites: ●, feldspar phenocrysts set in green phonolitic glass; ○, feldspar phenocrysts in brown mafic glass. N, number of analyses.

higher sulphur (up to 0·9 wt % SO_3) and lower silica abundances (Fig. 8).

Poris Member

The Poris ignimbrite differs from other ignimbrites of Cycle 3 by its relatively low phenocryst content, and absence of macroscopic magma mingling textures (e.g. banded pumice) that is in part due to poor pumice preservation as a result of vapour-phase alteration. However, the occurrence of several compositionally distinct mineral phases is similar to other Cycle 3 ignimbrites. Feldspar phenocrysts are mostly homogeneous grains

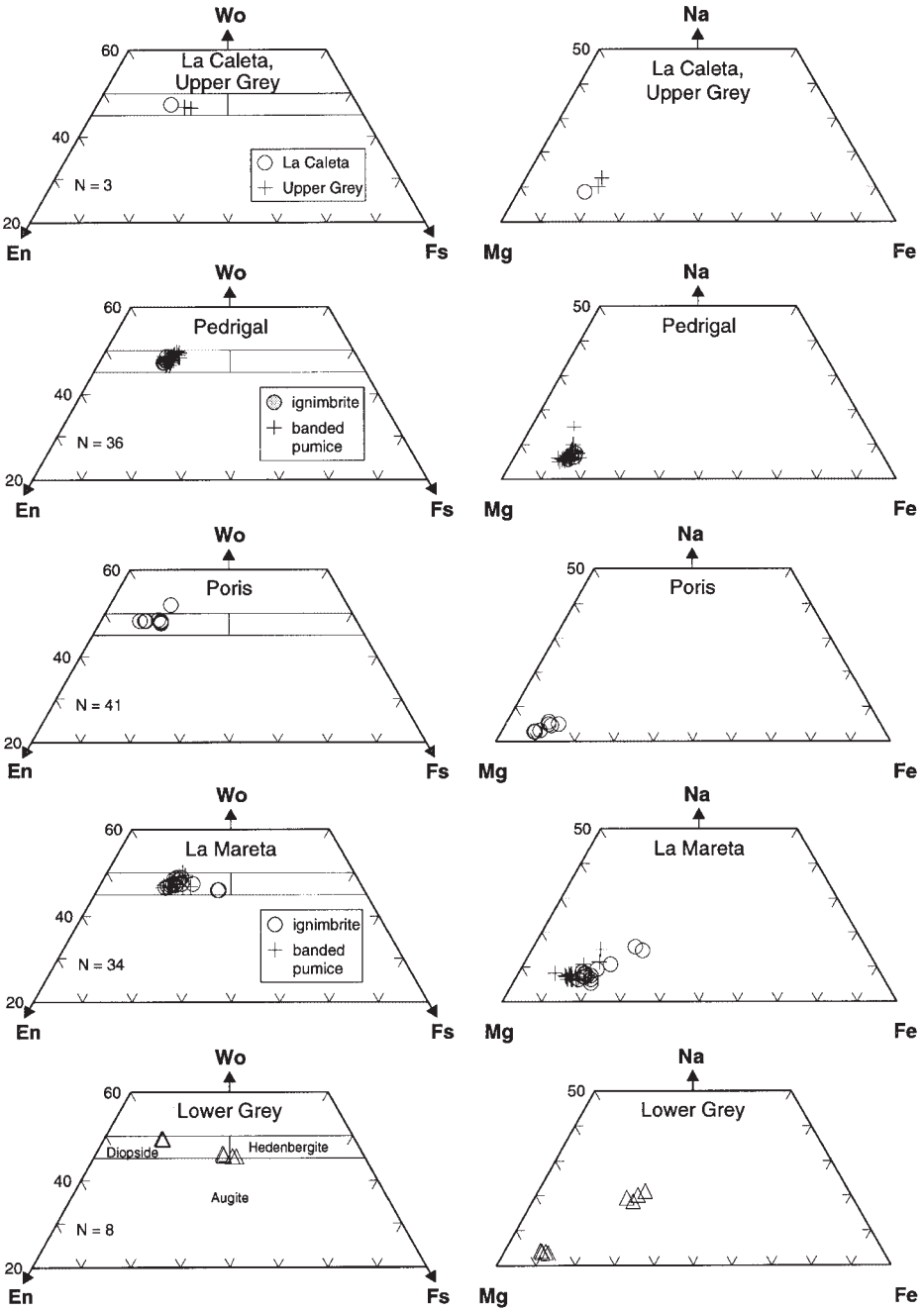

Fig. 13. Phenocryst pyroxene compositional variation of Cycle 3 phonolitic pyroclastic members, expressed in terms of the three-component system wollastonite (Wo)–enstatite (En)–ferrosilite (Fs); and Mg–Fe–Na (atomic per cent) relationships. Field boundaries after Morimoto (1988). N, number of analyses.

without significant zoning (Fig. 4), and are characterized by low Ba abundances. Three distinct feldspar populations can be defined (Fig. 12): sodic sanidine ($Ab_{57}An_2Or_{41}$), labradorite ($Ab_{39}An_{59}Or_2$) and a subordinate calcic andesine ($Ab_{53}An_{44}Or_3$) population. Diopsides have elevated Ti and Al abundances, and lack Na enrichment (Fig. 13). Two compositionally distinct titanomagnetite compositions occur, including an Al- and Mg-rich spinel and a Mn-rich titanomagnetite (Fig. 15).

Pedrigal ignimbrite

Banded pumice is particularly abundant in an ignimbrite cropping out locally in roadcuts between Abades and

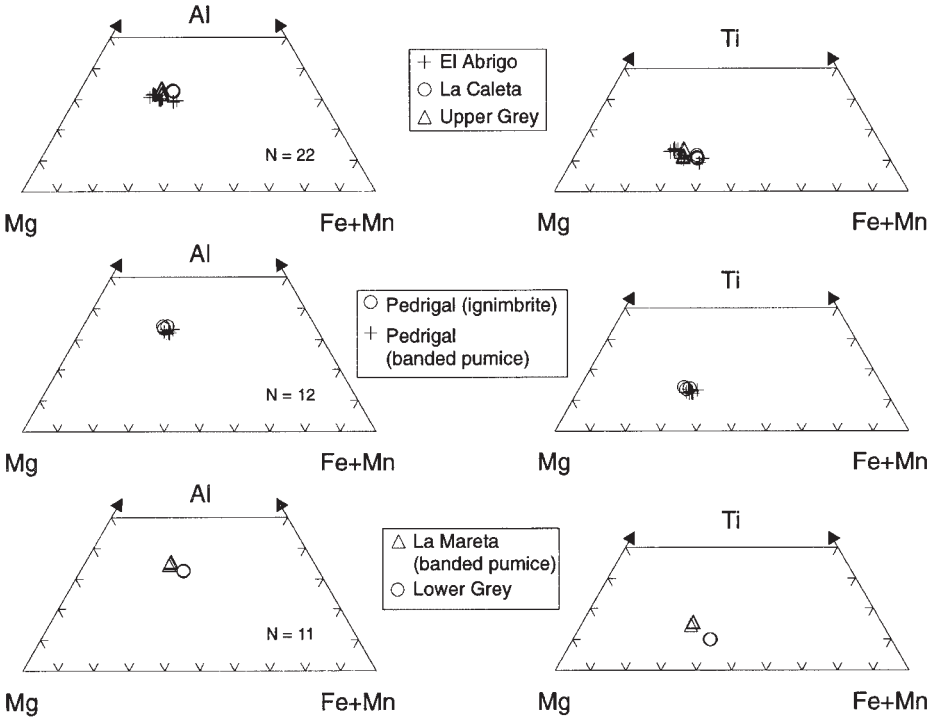

Fig. 14. Biotite phenocryst compositions (atomic per cent), Cycle 3 phonolitic pyroclastic members. N, number of analyses.

Poris de Abona (Fig. 1). The ignimbrite is informally named here the Pedrigal ignimbrite (after the nearby barranco), and the type locality of the ignimbrite is at $^{3}59^{320}$, $^{31}14^{230}$. The ignimbrite stratigraphically overlies the Poris Member, and is overlain by the Upper Grey Ignimbrite Member (Fig. 2). Three distinct pumice types are identified: (1) a crystal-rich, moderately vesicular, brown, glassy pumice with kaersutite, plagioclase, diopside and Fe–Ti oxides; (2) a crystal-poor, highly vesicular pumice, containing large phenocrysts of alkali feldspar, with lesser biotite, titanomagnetite and titanite; (3) banded pumice representing a mingling of the two. In banded pumice clasts, contacts between phonolitic and mafic glass are sharp, although brown streaks and wisps of mafic glass are distinctive in the phonolitic glass and indicate incomplete mixing of the two. The phonolitic glass is notably poorly vesiculated in the banded pumice clasts, and contains a diverse phenocryst assemblage of alkali feldspar, biotite, kaersutite (both as microphenocrysts and flow-aligned microlites), sodian diopside, titanomagnetite (with apatite inclusions), titanite and pale blue haüyne. The brown glass component of banded pumice clasts is similar to the crystal-rich pumice type, containing large kaersutite, plagioclase and titanian diopside phenocrysts. Kaersutite phenocrysts are generally rounded, with some enveloping augite cores.

Feldspar compositions are complicated by the presence of several distinct populations (Fig. 12)—sodic sanidine–potassic anorthoclase ($Ab_{54}An_1Or_{45}$–$Ab_{63}An_4Or_{33}$), anorthoclase ($Ab_{67}An_{11}Or_{22}$) and andesine–labradorite ($Ab_{58}An_{38}Or_4$–$Ab_{39}An_{59}Or_2$)—although a range of compositions between sodic bytownite and sodic labradorite ($Ab_{24}An_{75}Or_1$–$Ab_{48}An_{47}Or_3$) is observed in the banded pumice clast. The plagioclase feldspars are commonly resorbed, and anorthoclase feldspars have the highest Ba contents (up to 1 wt % BaO). Strong normal zoning characterizes some plagioclase phenocrysts (Fig. 4), whereas the alkali feldspars are mostly reversely zoned, reflecting the introduction of less mafic magma.

Diopsides from both mafic and phonolitic glasses are relatively uniform in composition (Fig. 13), show some reverse and normal zoning, and are characterized by relatively low Na contents, mostly ≤ 1 wt % Na_2O. Sodian diopsides as observed in other phonolitic pyroclastic members are notably lacking. Rare, homogeneous olivine grains ($\sim Fo_{80}$) with elevated CaO contents occur, and are similar in composition to olivine grains from other mixed phenocryst assemblage ignimbrites (Fig. 10). TiO_2 contents (6·2–7·2 wt %) are high and F abundances (<0·5 wt %) low for biotite phenocrysts. Kaersutite phenocrysts show little variation in Mg/(Mg + Fe) ratios and have negligible halogen contents (F + Cl $\leq$0·1 wt %), although there is some variation in tetrahedral Si:Al (Fig. 11). Tetrahedral Al is positively correlated with calcium content, suggesting increasing solid-solution of the Ca-Tschermak's component.

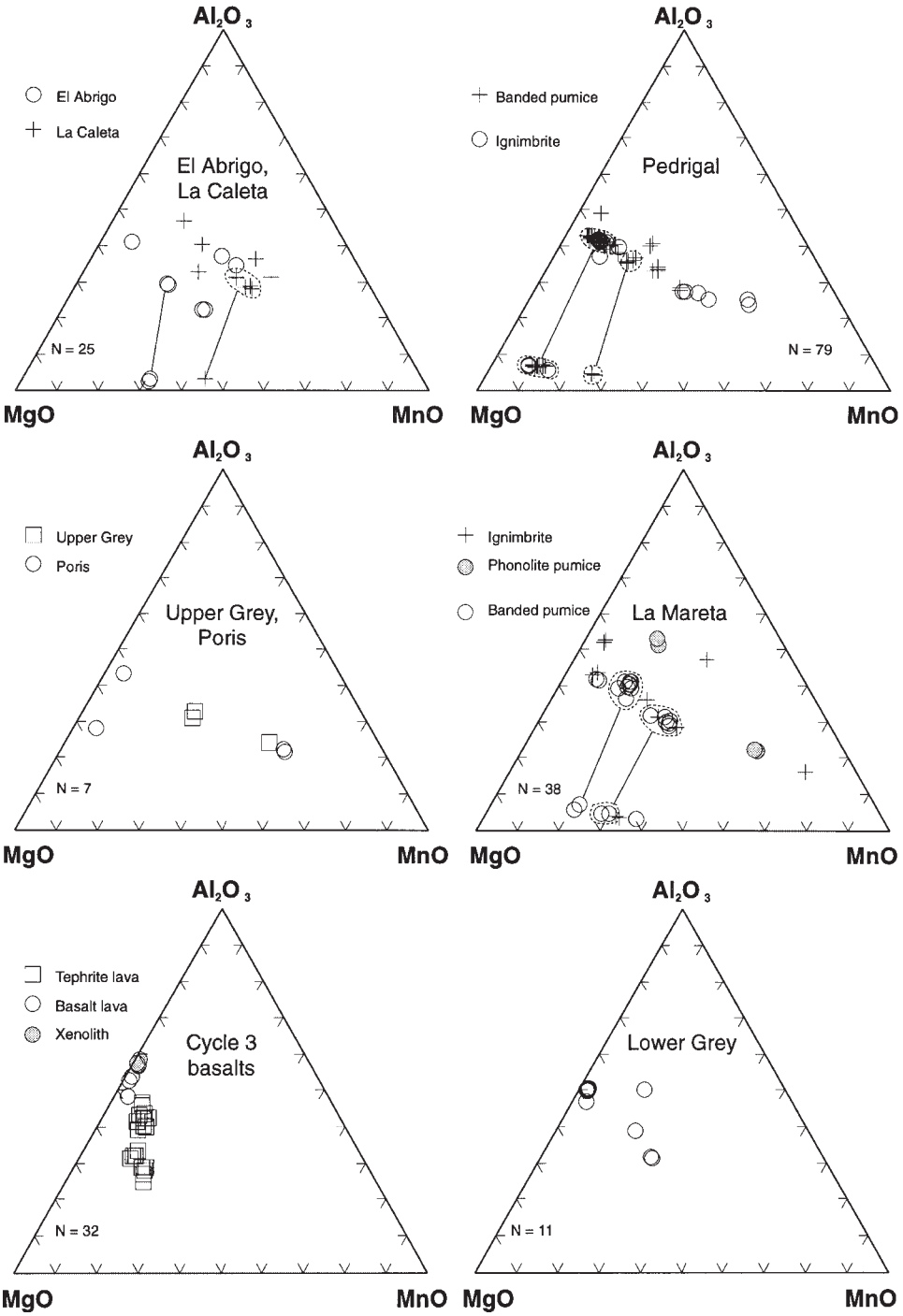

Fig. 15. Minor element compositions of coexisting titanomagnetite and ilmenite from lavas and phonolitic pyroclastic members of Cycle 3. Tie-lines join coexisting minerals interpreted to be in equilibrium. N, number of analyses.

Several distinct compositional populations of titanomagnetite occur, as observed in the other banded pumice-bearing ignimbrites (Fig. 15). Titanomagnetite crystal grains and inclusions within diopside phenocrysts are remarkably uniform in composition (Usp_{40-42}) and characterized by high Al_2O_3 and MgO contents. A subordinate Mn-enriched titanomagnetite population is also observed as liberated crystal grains in the ignimbrite matrix (Fig. 15). The two ilmenite populations in the banded pumices, differentiated by minor element

chemistry (Fig. 15), correspond to the mafic and phonolitic glasses. Apatite microphenocrysts mostly show intermediate abundances of SiO_2, SO_3 and F (Fig. 8). Haüyne phenocrysts (Fig. 9) are characteristically sulphur-rich ($\sim$9 wt % SO_3) and chlorine-poor.

Upper Grey Ignimbrite Member

The Upper Grey Ignimbrite is a relatively crystal-rich ignimbrite, containing a mixed phenocryst assemblage. Two pumice types are observed: (1) a moderately to highly vesicular, feldspar- and biotite-phyric pumice; (2) a brown, poorly vesicular pumice with abundant microlites of plagioclase. Apple green, sodian diopside crystal grains are distinctive within the ignimbrite matrix.

Although the Upper Grey and Lower Grey ignimbrites exhibit similar deposit characteristics (Bryan *et al.*, 1998), the two ignimbrites can be differentiated by mineral chemistry. Three distinct feldspar populations are identified (Fig. 12): sodic sanidine–potassic anorthoclase ($Ab_{51}An_1Or_{48}$–$Ab_{63}An_6Or_{31}$), anorthoclase ($Ab_{67}An_{13}Or_{20}$) and sodic labradorite ($Ab_{44}An_{53}Or_3$). Anorthoclase feldspars occur as phenocrysts within the moderately vesicular pumice clasts and contain the highest Ba contents ($\sim$0·6 wt % BaO). The alkali feldspar phenocrysts are normally zoned, whereas the plagioclase phenocrysts are reversely zoned (Fig. 4). Rare olivine grains in the ignimbrite matrix are notably more magnesian (Fo_{86}) than olivine analysed from other ignimbrites, and have correspondingly lower CaO contents (Fig. 10).

Biotite compositions are intermediate with respect to other phonolitic pyroclastic eruptive units in terms of TiO_2 (5·8–7 wt %), fluorine (0·3–0·55 wt %) and phlogopite (X_{phl} = 0·59) contents. Kaersutite phenocrysts are characteristically unzoned, and show little variation in Mg/(Mg + Fe) ratios (Fig. 11). A bimodality of kaersutite compositions is indicated, however, from Si:Al ratios (Fig. 11). The Al-rich kaersutites are also characterized by higher TiO_2, MgO and CaO, but lower F abundances.

Two titanomagnetite populations are observed, and lower ulvöspinel contents characterize titanomagnetite inclusions in diopside (Usp_{29}), compared with titanomagnetite grains (Usp_{37}) in the ignimbrite matrix. The titanomagnetite inclusions are also the most Mn-enriched (Fig. 15). Apatite is a common inclusion in titanomagnetite, and contains moderately high levels of silica (0·9–1·8 wt % SiO_2) but low sulphur ($\leq$0·1 wt % SO_3) contents (Fig. 8).

La Caleta Member

In the La Caleta ignimbrite, feldspar typically occurs as abundant, angular crystal fragments, although some show rounded corners and resorption. The feldspar grains in the ignimbrite matrix show a continuous range of compositions from calcic anorthoclase ($Ab_{70}An_{17}Or_{13}$) to potassic anorthoclase ($Ab_{60}An_4Or_{36}$). There are also subordinate populations of calcic oligoclase ($Ab_{68}An_{27}Or_5$) and sodic labradorite ($Ab_{44}An_{53}Or_3$; Fig. 12). A single phonolitic pumice clast within the ignimbrite was found to contain both calcic and potassic anorthoclase feldspars. The anorthoclase feldspars show only moderate Ba enrichment (<0·55 wt % BaO), but are characterized by extreme reverse and normal zoning patterns (Fig. 4). Both Ti-rich diopside and pale green, sodian diopside are present as liberated crystal grains in the ignimbrite matrix. Homogeneous biotite phenocrysts have relatively low TiO_2 (5·5–6 wt %), F (0·35–0·55 wt %) and phlogopite (X_{phl} = 0·55) contents. Individual kaersutite phenocrysts range from euhedral to subhedral and resorbed forms, are unzoned, but collectively show some variation in composition (Fig. 11): e.g. TiO_2 (4–6·6 wt %), and MnO (0·15–0·65 wt %). Halogen occupancy of the hydroxyl site is typically low (<0·2 a.f.u.).

Titanomagnetite and ilmenite occur as microphenocrysts within pumice and as crystal grains within the ignimbrite matrix. Ulvöspinel solid-solution varies from Usp_{27} for inclusions within biotite to Usp_{40} for microphenocrysts in pumice clasts. The ulvöspinel content of titanomagnetite grains in the ignimbrite matrix spans the range between these two ulvöspinel contents. The titanomagnetite inclusions within biotite are poorer in minor elements, but more enriched in MnO than microphenocrysts in pumice. Coexisting ilmenite (Ilm_{85}) is relatively Mn-enriched, compared with ilmenite compositions from other phonolite pyroclastic units of Cycle 3 (Fig. 15).

El Abrigo Ignimbrite Member

The El Abrigo Ignimbrite represents the youngest caldera-forming phonolite pyroclastic eruption of the Las Cañadas volcano (Martí *et al.*, 1994; Bryan *et al.*, 1998). It contains a mixed phenocryst assemblage, and in places, banded pumices are observed in the middle to upper parts of the ignimbrite. Three distinct compositions of feldspar are present (Fig. 12): sodic sanidine to potassic anorthoclase ($Ab_{60}An_1Or_{39}$–$Ab_{65}An_5Or_{30}$), anorthoclase ($Ab_{71}An_{11}Or_{18}$) and calcic oligoclase ($Ab_{67}An_{28}Or_5$). The oligoclase and anorthoclase phenocrysts are both resorbed and have high Ba abundances (up to 0·9 wt % BaO). Alkali feldspar grains within the ignimbrite matrix rarely exhibit resorption textures, and most are normally zoned (Fig. 4). Two biotite compositions can be distinguished, based on Ti content (<6 wt %, and $\sim$7 wt % TiO_2). The biotites lower in Ti are relatively Fe-enriched with higher Mn and F (up to 1 wt %), but lower Al and Ba abundances. The phlogopite component varies from 0·54 to 0·63, and the biotites are notable for almost complete occupancy of the X site (Ca + Na + K + Ba $\approx$ 1). Minor kaersutite grains have a relatively high

proportion of tetrahedral Al (lower TSi, Fig. 11), and are weakly normally zoned. Halogen substitution in the hydroxyl site of the kaersutites is negligible (<0·1 a.f.u.).

Coexisting Fe–Ti oxides are present and, as in other phonolites, ilmenite is subordinate to titanomagnetite. Variation in minor element behaviour (Fig. 15) shows the presence of several compositionally distinct titanomagnetite phases, but the minor element chemistry has been affected by some subsolidus equilibration (Fig. 15). Ulvöspinel solid-solution ranges from 37 to 42%.

Lavas

Cycle 2 phonolitic lavas

Phonolite lava of Montaña Guaza (Fernández-Santin & López, 1978; Fig. 2) contains abundant, ragged phenocrysts of alkali feldspar, with microphenocrysts of Fe–Ti oxides, and diopside to pale green, sodian diopside. Hydrous phases (biotite or kaersutite) are notably absent.

The phonolitic lava exposed in the Barranco de Charcon ($^{3}48^{400}$, $^{31}08^{700}$; Fig. 2) contains rare microphenocrysts of flow-aligned calcic anorthoclase ($Ab_{73}An_{10}Or_{17}$; Fig. 3), Fe–Ti oxides, and pale blue haüyne (partly altered), set in a trachytic-textured groundmass. Of note is the lack of chemical variation of feldspar compositions, and the generally higher Ba abundances (~0·45 wt % BaO) of the calcic anorthoclase feldspars than observed in the interbedded phonolitic pyroclastic members. Another weakly porphyritic, vesicular, phonotephrite to tephriphonolite lava underlying the Granadilla Member near Chimiche ($^{3}52^{819}$, $^{31}09^{448}$) contains a phenocryst assemblage of sodic plagioclase, diopside, Fe–Ti oxides, rare haüyne and kaersutite. Kaersutite is commonly anhedral and surrounded by a variably developed Fe–Ti oxide reaction rim, probably in response to water loss during eruption (e.g. Rutherford & Hill, 1993). The presence of sieved and skeletal plagioclase phenocrysts and abundant, black, irregular-shaped scoriaceous inclusions containing plagioclase ± kaersutite microphenocrysts, suggests magma mixing before eruption (e.g. Araña *et al.*, 1994).

Cycle 3 basalts

Cycle 3 basalt lavas represent widespread flank emissions that preceded the phonolitic explosive eruptions of Cycle 3 (Bryan *et al.*, 1998). The lavas are typically coarsely phenocrystic with olivine, titanian diopside, subordinate titanomagnetite ± groundmass plagioclase. Olivine exhibits occasional resorption and embayment, whereas titanian diopside commonly shows strong zoning patterns and brown (Ti-rich) rims. Some lavas contain xenoliths with subequal proportions of titanian diopside and olivine, with lesser Cr-spinel (olivine clinopyroxenite to wehrlite), and/or titanian diopside and spinel. Large crystal fragments (megacrysts, >1 cm diameter) of titanian diopside are common in these xenolith-bearing lavas. Wolff (1983) also reported mafic xenoliths from the tuff ring at El Medano ($^{3}51^{470}$, $^{31}04^{710}$).

Mg-rich olivine is characteristic ($Fo_{81–85}$), but is less magnesian than olivine in xenoliths (Fo_{87}, Fig. 10). Olivine phenocrysts are notably more calcic (>0·2 wt % CaO) than olivine in the xenoliths. Similar Ca enrichment and Ni depletion trends (Fig. 10) with decreasing forsterite content have been described from alkalic and tholeiitic basalts and xenoliths from Hawaii (Bohrson & Clague, 1988), and Tertiary tholeiitic to alkalic and nephelinitic basalts of eastern Australia (Ewart, 1989). Elevated calcium contents in olivines can be caused by either high iron content and/or high calcium concentrations in the melt (Jurewicz & Watson, 1988).

Titanian diopside phenocrysts ($Wo_{49}En_{38}Fs_{13}$) are generally distinguished by their buff pink colour in thin section. Diopside occurring in xenoliths ($Wo_{46}En_{48}Fs_{6}$) represents the most magnesian compositions so far analysed from the Bandas del Sur Formation (Fig. 16). Most diopside phenocrysts are weakly, normally zoned, but some are reversely zoned. Ti–Al relationships (Fig. 16) show a Ti:[Al^{4}] ratio of less than 1:2, and the excess Al has been related to increasing solid-solution of the Ca-Tchermak's component ($CaAlAlSiO_6$; Scott, 1976; Wolff, 1983). The solid-solution of the $CaCrAlSiO_6$ component may also be important in the Cr-rich diopsides (Fig. 16). Increasing Cr content correlates with increasing MgO [i.e. decreasing Fe/(Fe + Mn + Mg + Ca) values in Fig. 16]. Diopside phenocryst cores are generally enriched in Cr, compared with rim compositions, although some are notably reversely zoned. Maximum Cr levels are observed in pyroxenes of xenoliths, suggesting initial precipitation from primitive magmas. Some phenocrysts also exhibit high Cr abundances at slightly higher Fe ratios (Fig. 16). The diopsides of both phenocrysts and xenoliths show a sharp decrease in Cr over relatively small changes in Fe content.

Cr-bearing titanomagnetite (~5–7 wt % Cr_2O_3) and lesser titanomagnetite occur as phenocrysts in the basalt lavas, and Cr-rich (~38 wt % Cr_2O_3) spinels occur in xenoliths. A depletion trend in Cr is shown from the Cr-rich spinel (magnesiochromite) in xenoliths and alkali basalts to titanomagnetite phenocrysts in the tephritic and phonolitic lavas and pyroclastic rocks (Fig. 17), which links the $Mg(Al,Cr)_2O_4$–$Fe(Al,Cr)_2O_4$ and Fe_3O_4–Fe_2TiO_4 solid-solution end-members. The spinel phases in the xenoliths and as phenocrysts in the basalt lavas are characterized by extremely high MgO (6–14 wt %) and Al_2O_3 (6–16 wt %) contents (Fig. 15).

Cycle 3 tephrite to phonotephrite lavas

Minor, late-stage tephrite and phonotephritic lavas overlie the Cycle 3 basaltic lavas. The phonotephritic lavas are

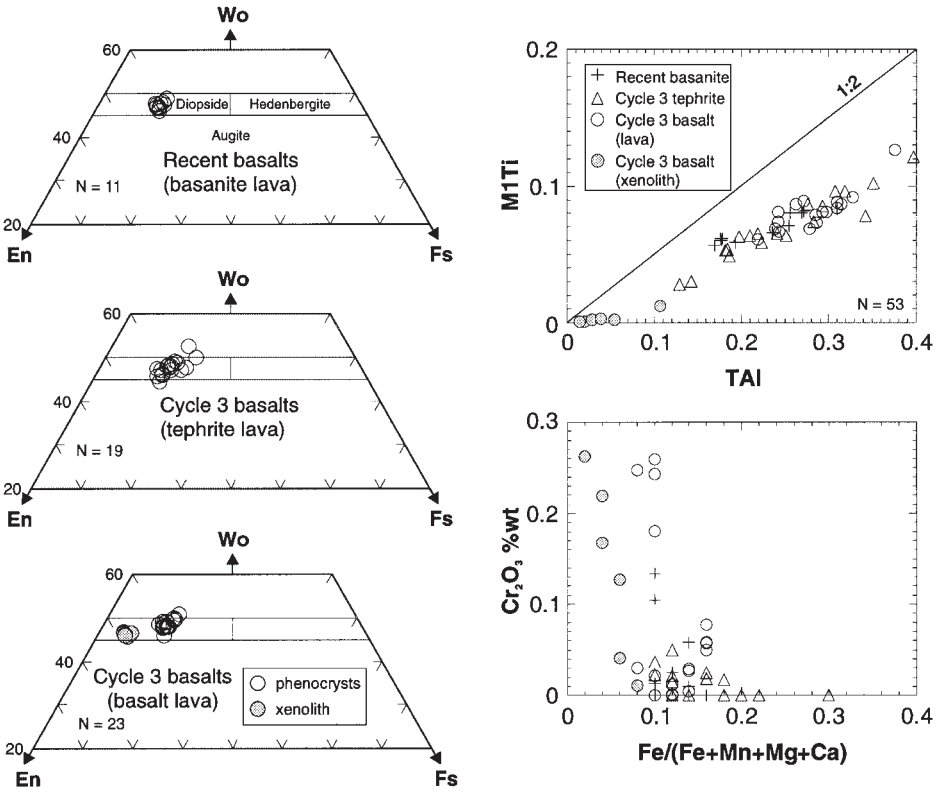

Fig. 16. Phenocryst pyroxene compositional variation of Cycle 3 basalts and Recent basalts expressed in terms of the three-component system wollastonite (Wo)–enstatite (En)–ferrosilite (Fs). Field boundaries after Morimoto (1988). Also shown are Ti:Al (O = 6) relationships and Cr_2O_3 content vs clinopyroxene composition (atomic per cent). The prefixes M1 and T denote cations in the octahedral and tetrahedral sites, respectively. N, number of analyses.

distinguished by the phenocryst assemblage plagioclase + kaersutite + diopside + titanomagnetite + apatite. Groundmass phases are dominated by subtrachytic-textured plagioclase, with lesser diopside and titanomagnetite. Kaersutite commonly exhibits a variably developed Fe–Ti oxide rim. Reaction rims to kaersutite are not observed in the pyroclastic units, and this suggests that those in lavas reflect dehydration of magma during relatively slow ascent to the surface (e.g. Rutherford & Hill, 1993). The presence of rare, highly corroded titanite phenocrysts, rimmed by oxide in one lava suggests pre-eruptive mixing with phonolitic magma.

The prominent tephrite lava near Tajao ($^{3}54^{796}$, $^{31}12^{033}$) contains only rare phenocrysts of diopside and microphenocrysts of feldspar, titanomagnetite, haüyne and apatite. Diopside phenocrysts extend from relatively magnesian compositions to compositions above the diopside–hedenbergite join ($Wo_{46}En_{41}Fs_{13}$–$Wo_{53}En_{32}Fs_{15}$). The diopsides show a wide variation in absolute TiO_2 (1–4 wt %) and Al_2O_3 (~3–9 wt %) contents, and corresponding Ti/Al values (Fig. 16). The consistently higher Al solid-solution levels in the phenocrysts (as observed in the basalts) may result from the higher total pressure effects during crystallization (e.g. Ewart, 1989). Cr contents in the diopside are typically low (Fig. 16). Titanomagnetite shows a range in ulvöspinel solid-solution ($Usp_{26–61}$), although microphenocrysts are mostly within the range of 46–57% ulvöspinel solid-solution. Titanomagnetite compositions are distinguished from those in the basalt lavas by higher MnO contents, and overall lower minor element abundances. Groundmass plagioclase is strongly zoned from labradorite ($Ab_{40}An_{58}Or_2$) to sodic andesine ($Ab_{63}An_{31}Or_6$; Fig. 12); plagioclase rim compositions are also higher in Ba (~0·2 wt % BaO). Apatite microphenocrysts and inclusions have higher F contents (up to 3·8 wt %) than those in the phonolitic pyroclastic units (Fig. 8a). Attention is also drawn to the moderately high sulphur (~0·5 wt % SO_3), chlorine (0·2–0·4 wt %), and low silica (~0·4 wt %) abundances of apatite (Fig. 8).

Recent basalts

The Recent basalts have similar phenocryst mineralogies to the Cycle 3 basalts. A range of compositions (basalt–basanite–phonotephrite) was erupted at the Valle San

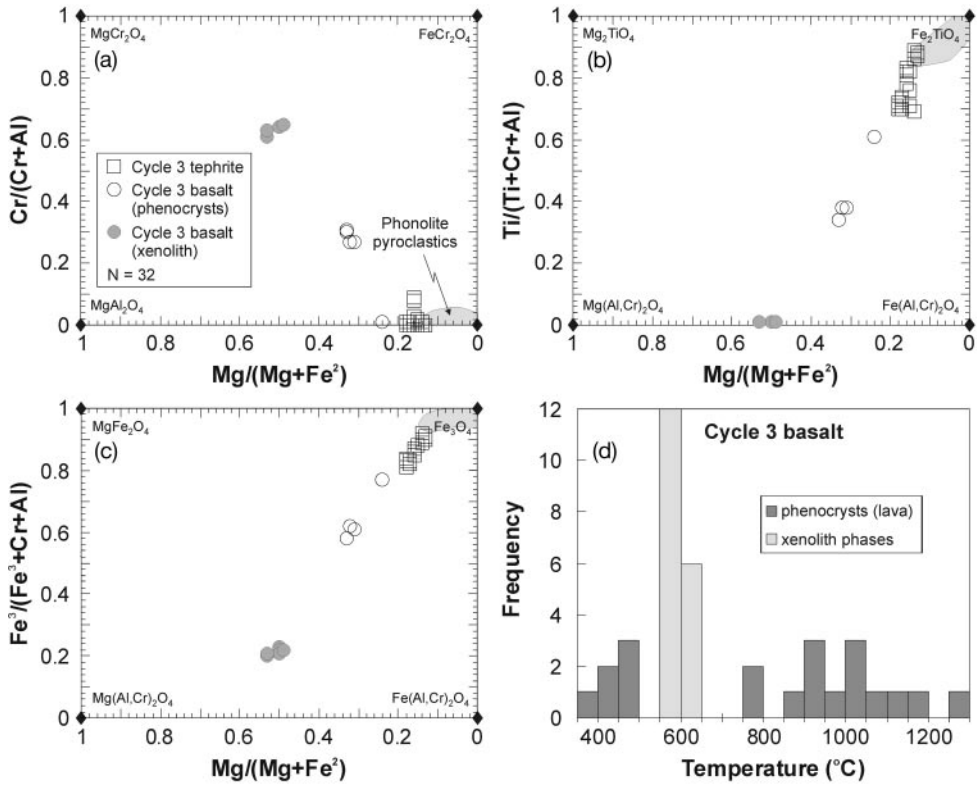

Fig. 17. (a–c) Cr-spinel and Cr-bearing titanomagnetite compositions (atomic per cent) for the Cycle 3 and Recent basalts. Shaded region represents titanomagnetite compositions of the phonolitic pyroclastic units. N, number of analyses. (d) Histogram of equilibration temperatures for Cycle 3 basalt lava (sample 76) calculated from coexisting olivine–Cr-spinel and Cr-bearing titanomagnetite pairs using the method of Roeder *et al.* (1979).

Lorenzo lava field in SW Tenerife. Some scoria cones contain phonotephritic scoria, with a phenocryst assemblage of diopside, plagioclase and rare kaersutite; olivine is absent. The associated lavas are more commonly basalts and basanites (Fuster *et al.*, 1968), containing phenocrysts of olivine, titanian diopside and titanomagnetite. Large olivine phenocrysts commonly show some resorption and embayment, and titanomagnetite inclusions are abundant in both olivine and diopside. Groundmass phases include abundant diopside, titanomagnetite and, rarely, plagioclase.

The basanite lava confined to the Barranco del Helecho near Las Vegas and Chimiche ($^{3}54^{240}$, $^{31}08^{511}$) has a slightly higher proportion of (titanian) diopside, and lacks the abundant and large (up to 1 cm diameter) olivine phenocrysts observed in the basalt lavas. Olivine phenocrysts are typically euhedral, although some exhibit embayment and resorption. Mg-rich olivines ($Fo_{74–87}$) are characteristic (Fig. 10), and some groundmass olivines represent the most Fe-enriched compositions. Olivine phenocrysts are generally normally zoned by up to 10% forsterite content, although some are reversely zoned. The olivines show a wide range of Ca and Ni solid-solution over a small range of Fe enrichment (Fig. 10), but completely overlap with olivine compositions from the basaltic lavas. The extension towards higher Ca contents occurs in phenocryst-rim and groundmass olivine. Diopside phenocrysts are relatively uniform in composition ($Wo_{47}En_{41}Fs_{12}$), and comparable with those in the Cycle 3 basalt lavas (Fig. 16). The lower Cr contents in diopside indicate that crystallization occurred from a more evolved magma composition than the basalts (Fig. 16).

Intensive parameters

Geothermometry and oxygen barometry

Temperature estimates for the phonolitic pyroclastic units are based on coexisting Fe–Ti oxides, and the biotite geothermometer of Luhr *et al.* (1984). Temperature and oxygen fugacity estimates from coexisting Fe–Ti oxides follow the method of Ghiorso & Sack (1991). The olivine–augite geothermometer of Loucks (1996) and the olivine–spinel geothermometer of Roeder *et al.* (1979) are used to provide temperature estimates for the basaltic lavas. The Fe–Ti oxide geothermometry has been cross-checked

Table 2: Summary of Fe–Ti oxide geothermometry and oxygen geobarometry for phonolitic pyroclastic units of the Bandas del Sur Formation

Sample	Member	% Usp	% Ilm	T (°C)	logfO_2	Comment
Cycle 3						
93A	El Abrigo Ignimbrite	37 (2)	86 (2)	932	−10·9	crystal grains in ignimbrite
62	La Caleta ignimbrite	34 (4)	85 (1)	883	−11·6	crystal grains in ignimbrite
122IG	Pedrigal ignimbrite	41 (7)	85 (3)	1013	−9·5	crystal grains in ignimbrite
122BP	Pedrigal ignimbrite	42 (32)	84 (11)	1045	−8·9	brown glass, banded pumice
122BP	Pedrigal ignimbrite	37 (11)	84 (2)	970	−10·2	green glass, banded pumice
93LMBP	La Mareta Ignimbrite	35 (6)	84 (1)	960	−10·3	green (phonolitic) glass
93LMBP	La Mareta Ignimbrite	39 (2)	81 (2)	1067	−8·4	brown glass (phonotephritic)
—	Tajao ignimbrite	38	85	915	−11·4	Wolff & Storey (1983)
Cycle 2						
6t	Granadilla ignimbrite	39 (2)	88 (1)	989	−10·0	crystal grains in ignimbrite
6r	Granadilla ignimbrite	31 (2)	93 (1)	793	−14·2	crystal grains in ignimbrite
8m	Granadilla pumice	34 (1)	93 (2)	804	−14·2	rim pairs; unit 4
8m	Granadilla pumice	33 (4)	90 (2)	864	−12·4	core pairs; unit 4
111b	Granadilla pumice	38 (4)	89 (4)	944	−10·7	unit 1
120IG	Abades Ignimbrite	43 (4)	86 (2)	1023	−9·4	crystal grains in ignimbrite
120MS	Abades Ignimbrite	42 (5)	86 (2)	1035	−9·1	brown glass, mafic pumice
128IG	Saltadero Ignimbrite	37 (4)	88 (4)	872	−12·4	crystal grains in ignimbrite
128MS	Saltadero Ignimbrite	38 (2)	87 (2)	910	−11·6	banded pumice clast

Numbers in parentheses denote number of analyses.

by several different and independent mineral thermometers (see Wolff & Storey, 1983; Bryan, 1998), which are in general agreement.

Minor element plots for Fe–Ti oxides (Figs 7 and 15) provide an indication of equilibrium vs disequilibrium coexisting compositions, based on tie-line slopes (Carmichael, 1967). As exemplified by the Granadilla and Abades members, most units show a spread of Fe–Ti oxide compositions, or contain evidence for more than one population. The usefulness of coexisting Fe–Ti oxides for temperature and oxygen fugacity estimates are therefore hindered by: (1) discordant coexisting Fe–Ti oxide pairs, observed in all pyroclastic units; (2) a corresponding lack of ilmenite analyses (ilmenite being subordinate to titanomagnetite); (3) the absence of ilmenite in the basaltic rocks and in some phonolites. Temperature and oxygen fugacity estimates for some pyroclastic members using coexisting oxide compositional groups, selected from tie-line slopes and checked for Mg–Mn equilibrium (Bacon & Hirschmann, 1988), are listed in Table 2 and illustrated in Fig. 18. The wide range of temperatures indicated is consistent with previous studies (e.g. Wolff & Storey, 1983; Wolff, 1985; see Table 2), and reflects the different magma compositions preserved within the phonolitic pyroclastic deposits (e.g. in banded pumices). Equilibration for the phonolitic pyroclastic members from Cycles 2 and 3 is just above the nickel–nickel oxide (NNO) buffer (~0·5 log unit). In T°C–fO_2 space, the phonolitic pyroclastic units are inclined slightly to natural oxygen buffer assemblages, suggesting a system closed to oxygen [compare Teide lavas of Ablay *et al.* (1995*b*)]. Fe–Ti oxide geothermometry for two banded pumice-bearing ignimbrites (La Mareta and Pedrigal) indicates a high-temperature magma component (~1050°C), and bimodal temperatures for the brown (mafic) glass of banded pumice clasts. In hand specimen and thin section, the brown mafic glass typically appears homogeneous.

Most coexisting Fe–Ti oxide data yield temperature estimates for the intermediate magmas (tephriphonolite–phonotephrite) of >900°C. Application of the biotite geothermometer potentially provides further temperature constraints for phonolite magma; Ablay *et al.* (1998) found biotite to be stable between 760°C and 900°C for the Teide–Pico Viejo volcanic rocks. Comparative histograms of calculated temperatures using the biotite geothermometer are shown in Fig. 19, and there is general agreement with the Fe–Ti oxide data. Relatively low temperatures (~730–760°C) are indicated for the

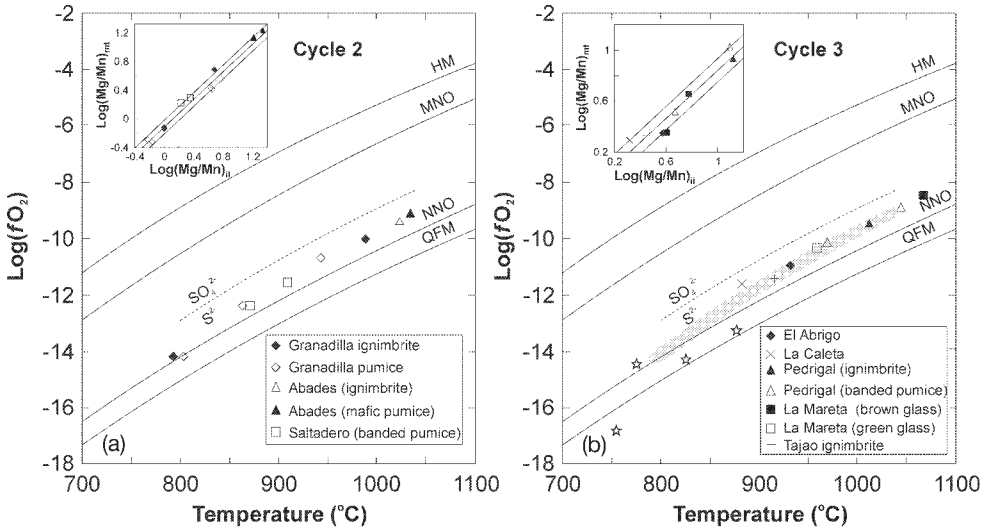

Fig. 18. Temperature–oxygen fugacity (fO_2) relationships obtained from coexisting Fe–Ti oxides for (a) Cycle 2 and (b) Cycle 3 phonolitic pyroclastic members of the Bandas del Sur Formation. Buffer curves from Rutherford (1993): HM, haematite–magnetite; MNO, MnO–Mn_3O_4; NNO, Ni–NiO; QFM, quartz–fayalite–magnetite. Inset figures show the Mg/Mn (atomic) distribution of oxide pairs used in geothermometry, compared with the equilibrium field of Bacon & Hirschmann (1988). In (b), the shaded region represents the field of T–fO_2 of Cycle 2 phonolitic pyroclastic members, and open stars represent T–fO_2 estimates for the ~2 ka Montaña Blanca eruption (Ablay *et al.*, 1995*a*). Data for Tajao ignimbrite from Wolff (1985).

plinian fall units of Cycle 2 (Unit E, El Rio). These temperatures are consistent with estimates from other Tenerife phonolites (e.g. Wolff, 1985; Ablay *et al.*, 1995*a*, 1998). Biotite geothermometry indicates a temperature of ~790°C for the phonolitic magma component in the Abades Ignimbrite (compare Fe–Ti oxide geothermometry, Table 2). Of note is the rise in equilibration temperatures between the last two plinian fallout units of Cycle 2 (El Rio and Granadilla pumice; Fig. 19). The generally higher Ti contents of biotites lead to higher equilibration temperatures for phonolitic pyroclastic members of Cycle 3, which is also indicated by the Fe–Ti oxide data. The very high temperature calculations (>1000°C) are from Ti-rich biotites occurring in the brown (mafic) glasses of banded pumice clasts (e.g. La Mareta Ignimbrite).

Results obtained from the olivine–augite geothermometer (Loucks, 1996) for the basaltic lavas yield comparable but slightly lower temperature estimates than those of Ablay *et al.* (1995*b*), who obtained temperatures between 1220 and 1180°C using Ca-in-olivine geothermometry (Jurewicz & Watson, 1988). Pairing of the most magnesian olivine and diopside compositions gave temperatures of 1195°C (core) to 1160°C (rim), whereas the most Fe-rich olivine–diopside pairs gave 1063°C (core) to 1051°C (rim). This might suggest a two-stage crystallization process for the basalts. Olivine and diopside phenocryst pairs from the Barranco del Helecho-confined basanite lava (Recent basalts) yielded temperatures of ~1140°C, with no discernible difference between core and rim compositional pairs. Groundmass olivine–diopside pairs, however, give lower temperature estimates of ~1080°C. Results from the olivine–spinel geothermometer (Roeder *et al.*, 1979), applied to Cr-spinel, Cr-rich titanomagnetite and coexisting olivine in the Cycle 3 basalt lava are shown in Fig. 17d. Only a few olivine–spinel pairs gave reasonable temperature estimates, suggesting some subsolidus equilibration affecting the Cr-spinels.

WHOLE-ROCK CHEMISTRY

Major and trace element geochemical analyses of pyroclastic members and lavas from the Bandas del Sur Formation are presented in Appendix A. Previously published data for Montaña Guaza (Fernández Santín & López, 1978), Caldera del Rey (Brandle, 1973), the Arico Ignimbrite (Schmincke & Swanson, 1967) and Recent basalts from the Valle San Lorenzo lava field (Fuster *et al.*, 1968) are also included in Figs 20 and 21.

The Bandas del Sur Formation comprises a diverse, but essentially bimodal suite of rock compositions, which form part of the series alkali basalt–basanite–phonolitic tephrite–tephritic phonolite–phonolite (Fig. 20). The Bandas del Sur volcanic rocks are alkaline (Fig. 20), and overlap with the range of compositions erupted from the post-caldera Teide–Pico Viejo stratovolcanoes (Ablay *et al.*, 1998). Alkali loss through weathering, post-eruptive hydration of pumices and/or vapour-phase alteration of

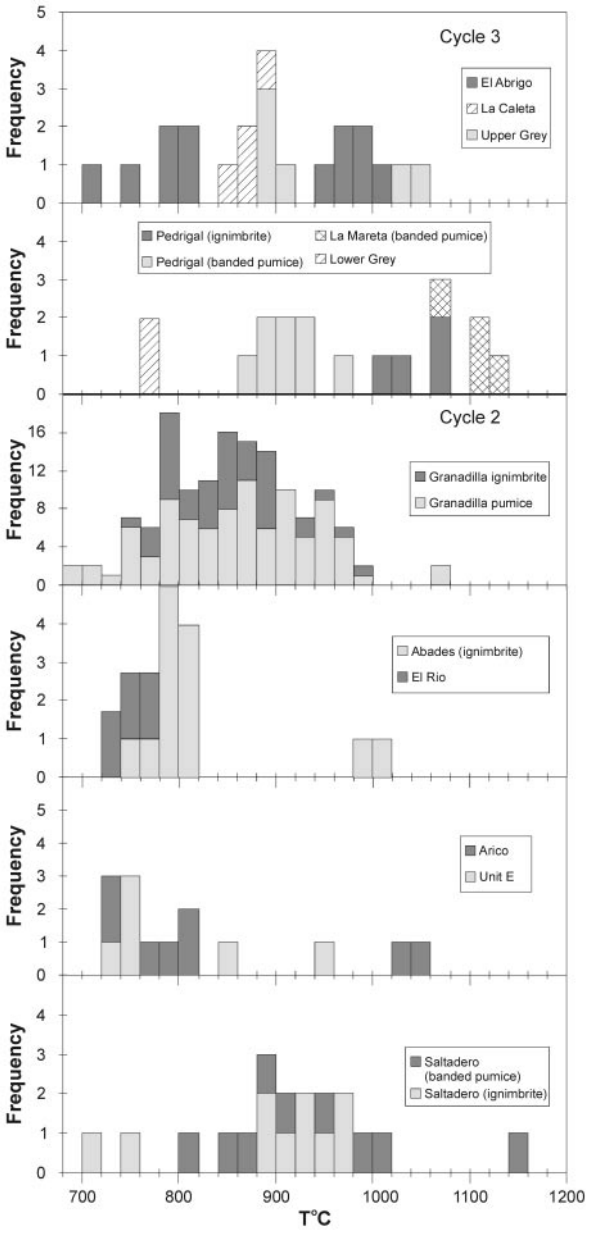

Fig. 19. Histograms of temperatures calculated using the biotite geothermometer of Luhr *et al.* (1984). Octahedral Ti instead of total Ti has been used in calculations. (Note the change in vertical scale for the Granadilla Member.)

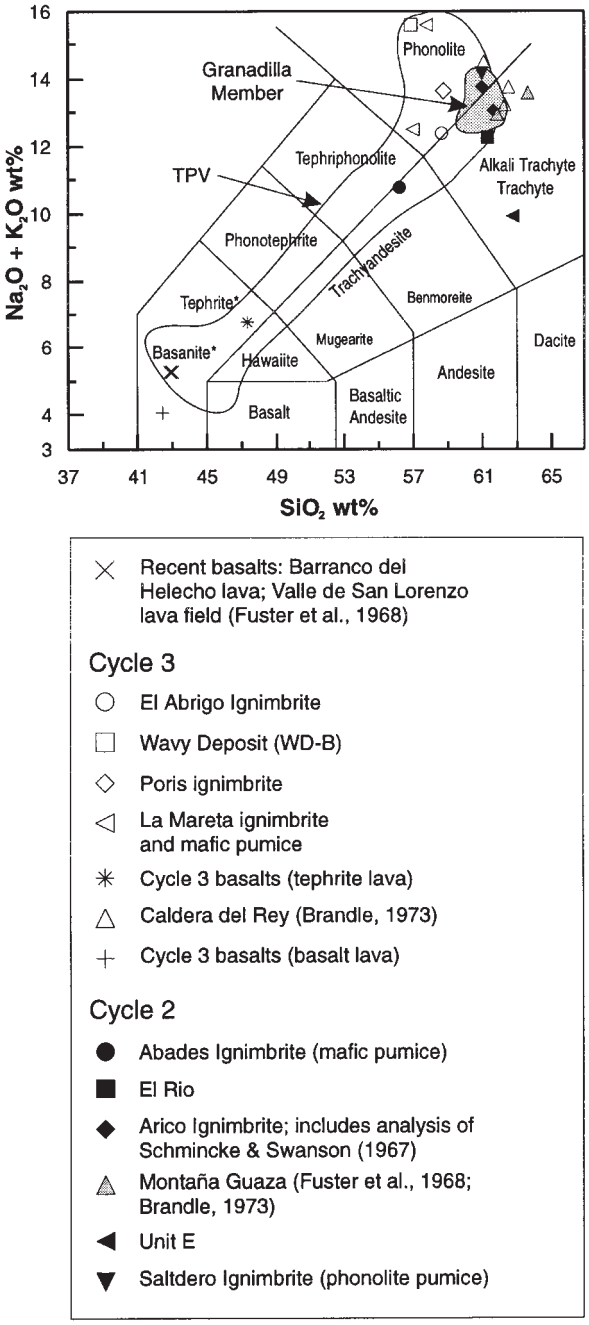

Fig. 20. Total alkalis–silica (TAS) plot (anhydrous basis) of selected units from the Bandas del Sur Formation. Field boundaries after Le Maitre (1989). *Basanite (modal olivine >10%); tephrite (modal olivine <10%). TPV, Teide–Pico Viejo stratovolcanic complex [data from Ablay *et al.* (1998)].

ignimbrite is interpreted to have affected some analyses (e.g. unit E of Fig. 20).

Major elements

Basaltic rocks

Significant differences are apparent between basanite (e.g. Recent basalts) and more primitive (e.g. Cycle 3 basalts) compositions, despite little increase in silica content (Fig. 21). Basanite lavas are notably enriched in TiO_2, Al_2O_3, CaO, Na_2O and P_2O_5, and show a relatively strong depletion in MgO. This is attributed to the removal of olivine, and is consistent with the slightly higher

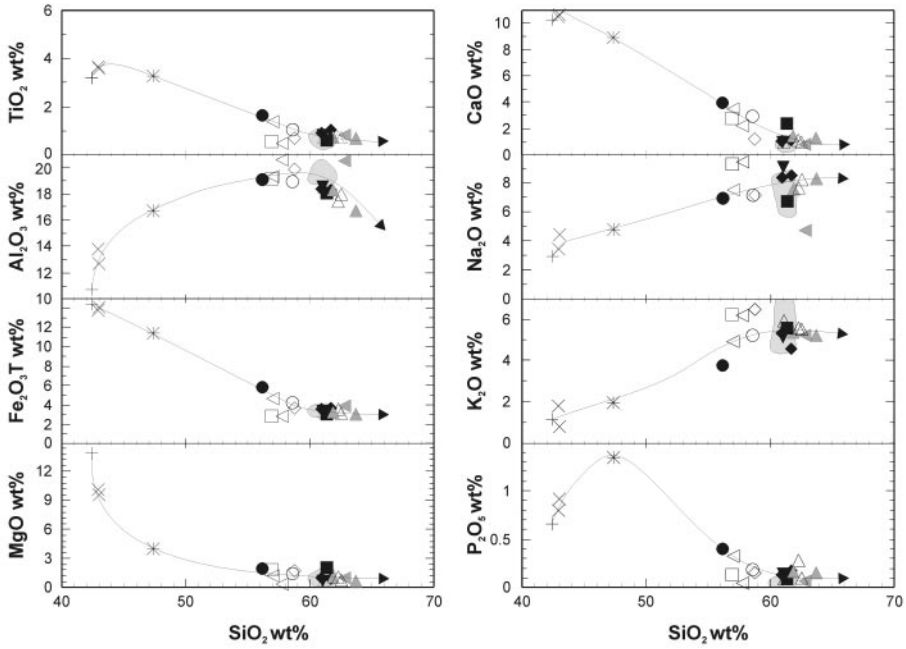

Fig. 21. Harker diagrams for the Bandas del Sur Formation. Symbols are the same as in Fig. 20. Shaded region represents compositions of the Granadilla Member (Bryan, 1998), and arrows illustrate enrichment or depletion trends of elements with increasing silica.

proportion of diopside observed in the basanite lavas. With continued fractionation toward tephritic compositions, TiO_2 becomes depleted, consistent with the removal of Fe–Ti oxides. Tephrite lavas have high P_2O_5 contents, which is reflected in the first appearance of apatite as a crystallizing (micro)phenocryst phase.

Phonolitic rocks

Alkalis and Al_2O_3 increase with SiO_2 until the phonolites ($\sim$58–63 wt % SiO_2), where Al_2O_3 decreases (Fig. 21) and K_2O/Na_2O increases. These features are compatible with alkali feldspar removal (see Ablay *et al.*, 1998). Phonolites show extreme depletions in TiO_2, MgO, CaO and P_2O_5 (Fig. 21), consistent with the removal of the observed phenocryst assemblages. In terms of Ca–Mg behaviour, there is a progressive, well-correlated depletion from the alkali basalts through to the phonolites. Of the analysed phonolites, Ca–Mg depletion is most pronounced in the Granadilla Member, suggesting that the culminating eruption of Cycle 2 tapped a large volume of highly fractionated phonolitic magma (Bryan, 1998).

Pumice glass

Selected electron microprobe analyses of glass in pumice have been given by Bryan *et al.* (1998). The complete dataset may be downloaded from the *Journal of Petrology* website at http://www.petrology.oupjournals.org. Glasses show a broad range of compositions from 51 to 63 wt % SiO_2 (Fig. 22). The brown (mafic) glass compositions of banded pumice clasts extend only to phonotephrite, and indicate that primitive basaltic magmas have not mixed directly with the capping phonolite magma. The glasses, like whole rocks, show well-defined, progressive depletions of Ca and Mg as silica increases, and depletions become most pronounced in the phonolite glasses (Fig. 22b). Of note is that pumice glass from the Granadilla pumice shows some of the most extreme depletions of Ca and Mg. Glasses are characterized by well-defined depletions or enrichments for most major and minor elements as silica increases (Fig. 22c). TiO_2, FeOT, MgO, CaO and P_2O_5 are progressively depleted with increasing silica, but have relatively flat trends above 60 wt % SiO_2. Like the whole-rock chemistry, the alkali elements and Al_2O_3 increase until the phonolites ($\sim$60 wt % SiO_2), but Ba shows a maximum in glasses between 54 and 55 wt % SiO_2. The depletion of Ba reflects its compatibility during the crystallization of oligoclase and calcic anorthoclase in the tephriphonolites (Fig. 22c). The mafic glasses notably have relatively high sulphur contents (Fig. 22c).

Trace elements

Basaltic rocks

Mid-ocean ridge basalt (MORB)-normalized trace element abundance patterns (Fig. 23) indicate that the

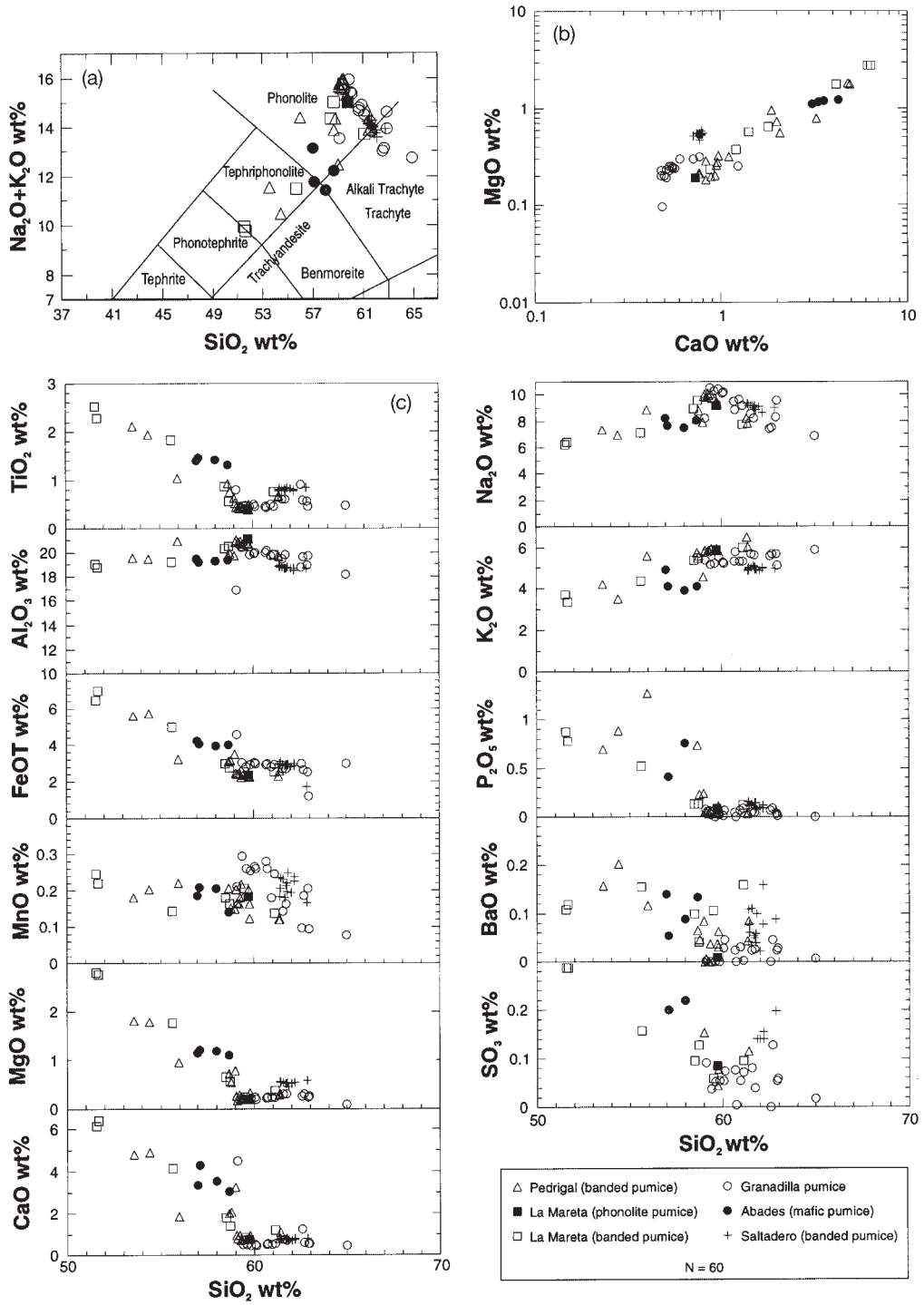

Fig. 22. Major element chemistry of pumice glass determined by electron microprobe. (a) TAS plot [field boundaries after Le Maitre (1989)]; (b) MgO–CaO relationships; (c) composite Harker diagrams (wt %). Glass analyses normalized to 100 wt %. N, number of analyses.

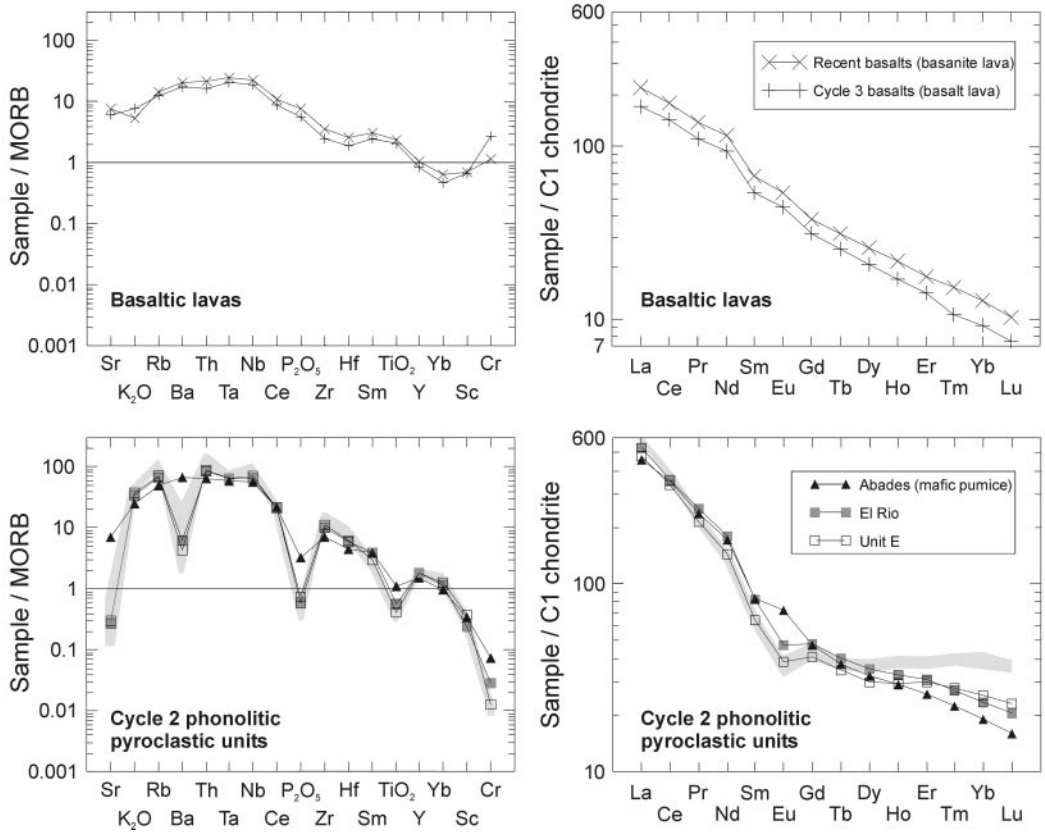

Fig. 23. MORB-normalized (Pearce *et al.*, 1981) spidergrams and chondrite-normalized (Sun & McDonough, 1989) rare earth element diagrams for selected pyroclastic members of Cycle 2, and Cycle 3 and Recent basalts. Shaded region denotes trace and rare earth element patterns of the Granadilla Member (Bryan, 1998).

basaltic lavas are relatively enriched in the incompatible elements from Sr to TiO_2, similar to those found in other intraplate environments (e.g. Pearce *et al.*, 1981; Cox, 1983; Ewart, 1989). A relative depletion is observed between Y and Sc; such depletions have been interpreted to reflect an inherited source characteristic in which garnet remained after partial melting. The basanite lava (Recent basalts) is characterized by higher absolute abundances of trace elements, compared with the Cycle 3 basalt, except Cr and K_2O. Cr depletion in the basanite reflects primarily the removal of Cr-spinel.

Sr and Ba exhibit a contrasting behaviour in the mafic and felsic rocks, increasing in abundance with Rb in the mafic rocks, but become progressively depleted as feldspars begin to dominate the fractionation assemblage (Fig. 24a and b). Sr content reaches a maximum in the tephrites, but the inflection from tephrite to phonotephritic compositions reflects the entrance of plagioclase. Maximum Ba enrichment (up to 1350 ppm) occurs in the tephriphonolites (Fig. 24b), but Ba becomes increasingly depleted in the phonolites as a result of feldspar removal. The high Ni abundance of the Cycle 3 basalt (Fig. 24c) suggests that it represents a relatively primitive magma. Increasing Sc with decreasing MgO content indicates little or no removal of diopside in the evolution of basanite from more primitive magmas. Olivine and diopside fractionation results in lower compatible trace element (Ni, Sc, Co, Cr) contents for the tephrite lava (e.g. Fig. 24d).

Phonolitic rocks

MORB-normalized trace element abundance patterns (Fig. 23) show that the phonolites are characterized by strong relative enrichments in the incompatible elements from K_2O to Nb, and superimposed depletions of Sr, Ba, P_2O_5, TiO_2, Sc and Cr. The Granadilla Member, by comparison, shows some of the strongest enrichment–depletion patterns. The tephriphonolites, represented by the mafic pumice from the Abades Ignimbrite Member (Fig. 23) are characterized by generally less pronounced enrichment in trace element abundances than the phonolites, particularly for K_2O, Rb, Th, Zr and Hf. The depletions of Sr, P_2O_5, TiO_2, Sc and Cr are also less than observed in the phonolites, and there is no relative depletion of Ba. The enrichment–depletion patterns of the phonolites indicate the importance of fractional crystallization in their evolution, and the strong depletions

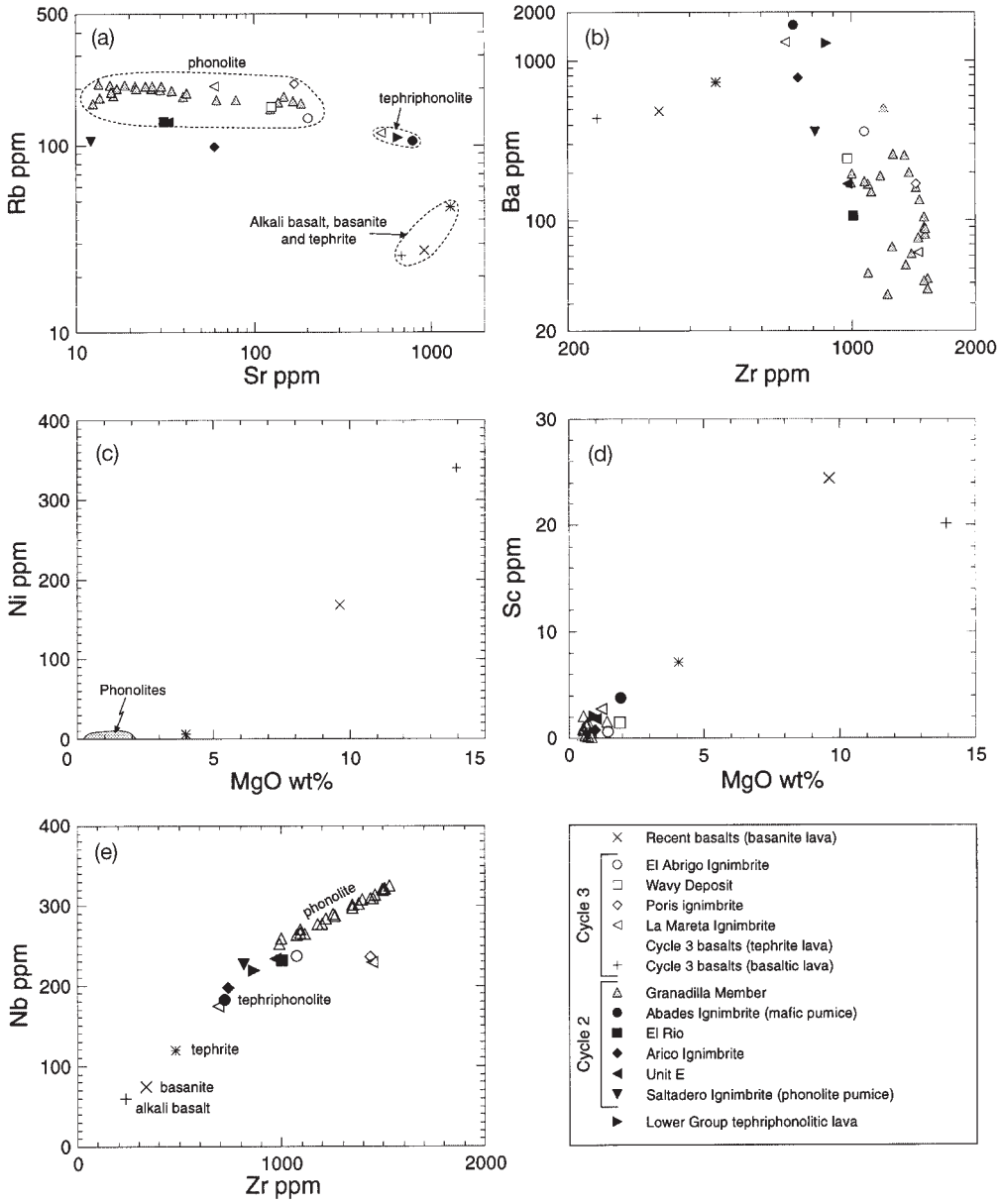

Fig. 24. Trace element characteristics of the Bandas del Sur Formation. (a) Rb vs Sr; (b) Ba vs Zr; (c) Ni vs MgO; (d) Sc vs MgO; (e) Nb vs Zr. Trace elements determined by XRF and normalized on a LOI-free basis.

in Sr, Ba, P_2O_5, TiO_2, Sc and Cr are qualitative evidence for feldspar, apatite, Fe–Ti oxide ($\pm$ biotite, titanite) and clinopyroxene fractionation, respectively. The small relative depletion in Ta, best observed in the Granadilla Member, is consistent with the removal of titanite (e.g. Wolff, 1984).

The extreme depletions of Sr and Ba in the phonolites (Fig. 24a and b) reflect plagioclase, followed by alkali feldspar (anorthoclase) fractionation, respectively. Zr–Nb relationships in the phonolites extend the positive trends observed in the mafic rocks (Fig. 24e). The slightly lower increase in Nb with Zr suggests some buffering of Nb by titanomagnetite removal.

Rare earth elements

Rare earth element (REE) abundances (Fig. 23; Table 3) in the basaltic rocks are characterized by relatively smooth and light REE (LREE)-enriched patterns, and higher REE abundances (relative to chondrite). Differing degrees of partial melting in the mantle source may

Table 3: Selected trace and rare earth element abundances and ratios

Sample	Member	Composition	La (ppm)	La_N/Sm_N	Tb_N/Yb_N	Eu/Eu*	La/Yb	Rb/Sr	Zr/Nb
50	Recent basalts	basanite	51·65	3·25	2·46	1·07	23·73	0·03	4·06
76	Cycle 3 basalts	basalt	40·46	3·19	2·75	1·10	25·71	0·04	3·46
Unit 1*	Granadilla	phonolite	140·23	10·82	0·92	0·69	25·16	5·36	4·19
Unit 3†	Granadilla	phonolite	139·34	11·80	0·94	0·65	26·62	8·20	4·33
Unit 4‡	Granadilla	phonolite	139·44	10·95	1·05	0·62	28·33	12·53	4·22
120MS§	Abades	tephriphonolite	109·08	5·45	1·95	1·15	33·42	0·12	3·34
43	El Rio	phonolite	114·75	7·55	1·36	0·75	26·28	3·81	4·10
18E¶	Unit E	phonolite	126·08	6·41	1·73	0·75	31·44	4·15	3·89

Normalized ratios based on C1 chondrite values of Sun & McDonough (1989). *Average of three samples. †Average of two samples. ‡Average of four samples. §Tephriphonolite pumice. ¶Pumice collected from middle of fall deposit.

explain the mostly uniform increase in REE abundance from alkali basalt to basanite (Fig. 23). Phonolitic pyroclastic members, in comparison, are strongly LREE-enriched (Fig. 23). The phonolites are characterized by a small to moderate Eu depletion ($Eu/Eu^* = 0{\cdot}79-0{\cdot}61$), which is consistent with depletions of other elements (Sr, Ba) that indicate feldspar fractionation. The tephriphonolite pumice of the Abades Ignimbrite, however, exhibits a positive Eu anomaly, suggesting feldspar accumulation (e.g. Stolz, 1985). Elevated heavy REE abundances and lower La/Yb values (Table 3) for the Granadilla Member are indicative of extended alkali feldspar dominated (e.g. $\geq$90 modal %, Ablay *et al.*, 1995*a*) fractionation.

DISCUSSION

The geochemical data presented here are consistent with previous studies that indicate that the evolution of Tenerife magmas from alkali basalt to phonolite is dominated by crystal–liquid fractionation processes. However, major, trace and rare earth element data imply a multistage evolution involving different fractionating mineral assemblages to account for the range of magma compositions (see also Ablay *et al.*, 1998). Despite the high Ni and Cr abundances, the basalt lavas (Cycle 3 and Recent basalts) do not represent primary magmas as they have accumulated phenocrysts of olivine and diopside. The Cycle 3 basalt lava does, however, represent the most primitive composition analysed from the Bandas del Sur Formation (e.g. Fig. 24c). Strong Mg, Ni, and less pronounced Cr depletion, coupled with increasing Nb, Sr and Sc, indicate that basanite magmas evolved from a parental basaltic magma primarily by the removal of olivine and Cr-spinel. Diopside then dominates the fractionating assemblage during crystallization from basanite to tephrite (e.g. Sc–Mg relationships, Fig. 24d). The addition of plagioclase and apatite, followed by kaersutitic amphibole (Ablay *et al.*, 1995*b*), to the fractionating assemblage determines the evolution of tephrite to tephriphonolite compositions. Phonolite evolution is controlled by alkali feldspar, but trace element behaviour also shows that other phenocryst phases (biotite, augite, Fe–Ti oxides, titanite and apatite) are important [see Ablay *et al.* (1998) for details of fractionation modelling].

Role of magma mixing

Although fractional crystallization appears to have been the overriding process in the development of the spectrum of Tenerife magma compositions (e.g. Ablay *et al.*, 1998), magma mixing and mingling processes are also important in determining the geochemical characteristics of individual phonolitic pyroclastic members (e.g. Wolff, 1985; Ablay *et al.*, 1995*a*). Magma mixing and mingling processes are recorded by the presence of mixed phenocryst assemblages and banded pumice clasts. Petrological relationships and mineral chemistry data provide strong evidence for both syn-eruptive mingling of phonolite and mafic (tephriphonolite–phonotephrite) magmas (e.g. banded pumice clasts), and an earlier (pre-eruptive) magma mixing event for the mafic magma component.

Mixing of basaltic and phonotephritic magmas

Pre-eruptive mixing of phonotephritic magma with basaltic magma is supported by the presence of anhedral olivine, bytownite and Cr-bearing titanomagnetite or two distinct Fe–Ti oxide populations (e.g. Abades, La Mareta,

Pedrigal ignimbrites). Fe–Ti oxide geothermometry indicates mixing involved basaltic and mafic tephriphonolitic magmas with temperatures in the range of 1050–1100°C and 950–1000°C, respectively.

The common presence of a basaltic component (e.g. bytownite, Cr-bearing titanomagnetite, olivine, titanian diopside) contradicts the conclusion of Wolff (1985) that this is 'atypical' for the phonolitic pyroclastic deposits of the Bandas del Sur Formation. Of significance, however, is that a basaltic component has so far been identified only in ignimbrites (e.g. Arico, Abades, Tajao, La Mareta, Pedrigal, Upper Grey), whereas the plinian pumice fallout deposits appear to lack a basaltic fingerprint. The 'ignimbrite-only' eruptive style may be in part related to the mixed magma characteristics and the processes involved; that is, the lower volatile contents of the mafic and intermediate magmas may be insufficient to support a buoyant and stable plinian column.

Wolff (1985) proposed several mechanisms to explain the early mixing of basaltic magma with overlying intermediate magmas (phonotephrite–tephriphonolite). His preferred model involves the crystallization and volatile saturation of basaltic magma injected into the base of the chamber, resulting in buoyant rise into, and thorough mixing with, intermediate composition magma. This model was based on the assumption that the calcic plagioclase compositions reflected crystallization under high P_{H_2O}. Alternatively, Ablay (1997) concluded that the precipitation of calcic plagioclase in basaltic rocks indicates crystallization at high P_{total} without the need for felsic contaminants or high P_{H_2O}.

An intriguing temporal relationship exists between phonolitic explosive volcanism of Cycles 2 and 3, and basaltic volcanism along the Dorsal Ridge (Fig. 1). Evidence for the contemporaneity of basaltic and phonolitic eruptions is provided by the interbedded nature of basaltic lavas and pyroclastic deposits with phonolitic pyroclastic deposits in the Diego Hernández Formation (Mitjavila, 1990; Martí *et al.*, 1995) of the caldera wall, and along the flanks of the Dorsal Ridge. Magma mixing may ultimately reflect the repeated interaction of basaltic magma from the Dorsal Ridge system with the phonolitic magma chamber(s) of the Las Cañadas volcano. It remains unclear whether the intrusion of basaltic magma triggered the latter mingling of phonolitic and tephriphonolitic magma, and subsequently eruption (i.e. domino effect), or if this earlier mixing event occurred in isolation. One constraint is that there must have been sufficient time between the two mixing events to allow almost complete hybridization of the mafic magma. The petrology and mineral chemistry therefore record complex, multistage histories involving multiple magma types for the banded pumice-bearing ignimbrites of the Bandas del Sur Formation.

Syn-eruptive mingling with phonolite magma

The characteristic banded or streaky pumice textures evident in pumice clasts result from a mingling event between phonolite and the hybridized mafic magma. Glass domain contacts are typically irregular but sharp. Wisps or streaks of brown glass, prominent in the marginal zones of phonolitic glass, describe complex mingling and incomplete mixing between the hybrid mafic and phonolitic melt. Blebs of mafic glass and xenocrysts are more common in the phonolitic glass, whereas the mafic glass is mostly free of phonolitic phenocryst phases. The generally sharp contacts between hybrid and phonolitic glasses in banded pumice and the lack of significant homogenization suggest mingling in the conduit just before, or during, eruption (e.g. Blake & Campbell, 1986; Druitt *et al.*, 1989).

Many phonolitic pyroclastic members of Cycle 2 lack the distinctive banded pumice and macroscopic evidence for commingling. However, banded pumice textures are observed, and are defined more by nonvesiculated and vesiculated, pale green glass domains in pumice clasts, and, in places, different associated phenocryst assemblages. There is little or no observable difference in glass colour and only subtle differences in glass major element chemistry. Commingling ($\pm$ mixing) between phonolite and less evolved phonolite to tephriphonolitic magmas may be a common, if not obvious process in the phonolitic pyroclastic members of Cycle 2.

Role of assimilation and fractional crystallization

Assimilation and fractional crystallization (AFC) processes were considered by Wolff & Palacz (1989) to be important in the evolution of three phonolitic pyroclastic units of Cycle 2. This was based on field and geochemical data; in particular, incompatible element behaviour and Pb isotope variation. The three units [the Granadilla Member, unit E, and another pumice fallout deposit—unit D of B. Booth & G. P. L. Walker (unpublished data collected in the 1970s), which underlies unit E; see Fig. 2] were considered comagmatic in the sense that they were all derived from the same high-level zoned magma chamber, shared a common parental magma, and followed closely similar crystallization paths (Wolff & Palacz, 1989). A comagmatic relationship was based on: (1) an apparent stratigraphic 'proximity'; (2) radiocarbon age data (Shotton & Williams, 1971; Booth, 1973) indicating repose periods of ≤ 1 kyr between eruptions; (3) a similarity in geochemical trends and trace element behaviour. However, all Tenerife magmas can be considered comagmatic in the sense that they are ultimately derived from the same parental basaltic magma composition, as

indicated by incompatible and compatible trace element plots (Fig. 24) for the Bandas del Sur Formation.

Contrary to the description of Wolff & Palacz (1989), several major phonolitic pyroclastic members separate unit E and the Granadilla Member (e.g. Arico and Abades ignimbrites), as well as deposits of many smaller eruptions (Bryan *et al.*, 1998). Stratigraphic information also indicates that larger volume eruptions occurred towards the end of Cycle 2 (e.g. Abades, Granadilla). Recent K/Ar age dating (Ancochea *et al.*, 1990; Bryan *et al.*, 1998) has since shown that the ages of eruption indicated by the radiocarbon age data are grossly inaccurate. A 'comagmatic' relationship is therefore not supported by field relationships, stratigraphic information or age data.

The strongest evidence cited by Wolff & Palacz (1989) for AFC processes was incompatible element behaviour. A plot of two highly incompatible trace elements obeying the Rayleigh fractionation law and having the same partition coefficients should yield a straight line that passes through the origin (Wolff & Palacz, 1989). Linear trends with non-zero intercepts between two incompatible elements provide a strong indicator of AFC (Powell, 1984). The incompatible trace element plots used by Wolff & Palacz (1989) to show non-zero intercepts are reproduced in Fig. 25. Both the data of Wolff & Palacz (1989) and new inductively coupled plasma mass spectrometry (ICP-MS) trace element data of this study are plotted, and the new data, which include basaltic rocks, clearly show zero or near-zero intercepts (Fig. 25). This excludes incompatible element plots using Zr or Hf, for which non-zero intercepts occur. As noted by Wolff & Palacz (1989), there is also a curvature of trends (e.g. U–Zr; Nb–Th; Fig. 25b) that may reflect changing partition coefficients during fractionation, and cause non-zero intercepts for linear regression lines. Nevertheless, the new data, encompassing a wider range of magma compositions, do not provide the compelling evidence for AFC as illustrated by Wolff & Palacz (1989). Additional analyses of other pyroclastic and lava units from the Bandas del Sur Formation are therefore required to better constrain the linear (or curved) trends on incompatible–incompatible trace element plots.

Comparison of the geochemical characteristics of Cycles 2 and 3

Two long-term cycles of phonolitic explosive volcanism identified for the Bandas del Sur Formation (Cycles 2 and 3 of Fig. 2) have been distinguished by field relationships, eruptive styles and deposit characteristics (Bryan *et al.*, 1998). The above outline of the mineral, major and trace element chemistry of the pyroclastic members also emphasizes differences between the two explosive cycles.

Cycle 2 (0·85–0·57 Ma)

Previous geochemical studies (e.g. Wolff & Storey, 1984; Wolff & Palacz, 1989) indicate several eruptions tapped chemically, and probably thermally stratified magma systems to produce plinian-type pumice fall deposits. This zonation is reflected by subtle variations in mineral, trace ± minor element chemistry, often at constant silica content (e.g. Granadilla Member, Wolff & Storey, 1984; Bryan *et al.*, 1998). Geothermometry (Figs 18 and 19) and trace element abundances of the pumice fallout deposits also indicate that the eruptions tapped relatively cool (≤800°C) and highly evolved phonolitic magma. Strongly Mn-enriched titanomagnetite compositions characterize these units (Fig. 7).

Not only have successive eruptions tapped larger magma volumes during the cycle, but compositional relationships of whole-rock (Rb–Th, Ba–Rb, Nb–Zr, Eu/Eu*; Fig. 24; Table 3) and, in particular, glass chemistry (e.g. CaO–MgO, Fig. 22b) indicate that the most fractionated phonolitic magma was tapped at the end of the cycle (Granadilla Member).

Magma mingling or mixing processes are evident in only a few pyroclastic deposits of Cycle 2 (e.g. Saltadero, Arico and Abades ignimbrites), and generally involved tephriphonolitic magmas. Further detailed studies are required to determine if other phonolitic pyroclastic deposits exhibit similar mineral and chemical heterogeneity to the Granadilla Member (Bryan, 1998). Of significance, however, is that the Abades Ignimbrite Member is the only member of Cycle 2 that preserves a strong basaltic magma fingerprint. Trimodal feldspar (Fig. 3) and bimodal compositions for other phenocryst phases (e.g. Fig. 7) within the characteristic black, mafic pumice clasts suggest a complex history of magma mixing ± mingling between basaltic, phonotephritic and phonolite magmas. The Abades Ignimbrite Member is important because it records a major recharge event just before the caldera-forming eruption of the Granadilla Member that ended the explosive cycle (see Wolff & Palacz, 1989).

Cycle 3 (0·37–0·17 Ma)

Banded pumice and/or mixed phenocryst assemblages characterize all units of the youngest cycle (Bryan *et al.*, 1998). Two distinct mixing events can be identified in several banded pumice-bearing ignimbrites, which record (1) a pre-eruptive mixing event between basaltic and phonotephritic–tephriphonolitic magmas and (2) mingling ± mixing between the hybrid mafic magma and phonolite. The repeated replenishment of the magma chamber system by basaltic magmas may be due to the proximity of phonolitic magma chamber(s) at the eastern side of the Las Cañadas caldera (i.e. as preserved in the

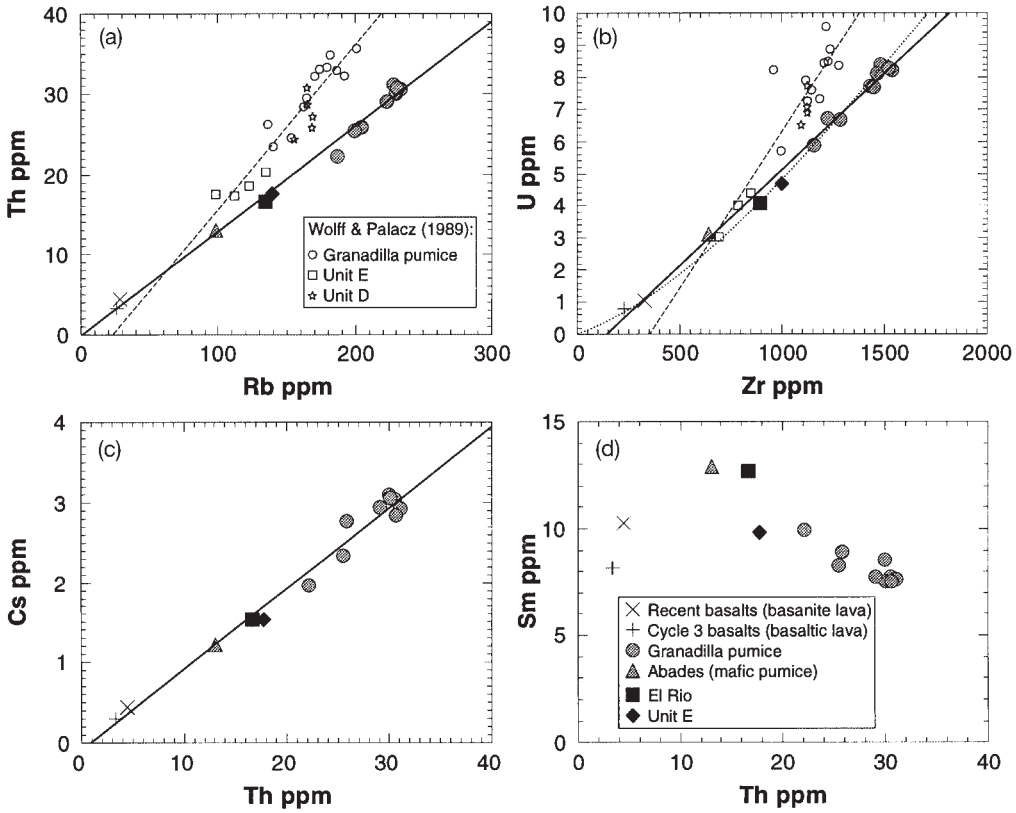

Fig. 25. (a–c) Incompatible–incompatible trace element plots. The Th–Rb and U–Zr plots were used by Wolff & Palacz (1989) to demonstrate non-zero intercepts for regression lines (dashed), which are indicative of AFC processes (Powell, 1984). Note: (1) linear regression lines for the new ICP-MS data for basaltic lavas and phonolitic pyroclastic units exhibit zero or near-zero intercepts; (2) the slight curvature in some element trends [dotted line in (b)]. Data and regression lines of Wolff & Palacz (1989) are shown in (a) and (b). (d) Sm (compatible) vs Th (incompatible) plot. Sm is initially incompatible in the mafic volcanic rocks, but behaves compatibly in the phonolites, as a result of titanite crystallization (Wolff, 1984).

Diego Hernández Formation) to the basaltic Dorsal Ridge system (Fig. 1).

The presence of any cryptic compositional zonation, as typified by the plinian fall deposits of Cycle 2, may be masked by the mingling and mixing events involving more mafic magmas. Geothermometry indicates that the phonolite magmas mostly remained hot ($\geq$900°C) and that substantial volumes of cooler ($\leq$800°C), highly fractionated phonolite magma did not accumulate during Cycle 3. Repeated recharge events may have maintained the elevated temperatures and/or prematurely triggered eruption, and therefore prevented significant volumes of cooler phonolite magma from accumulating at the top of the chamber by *in situ* fractionation.

Attention is also drawn to the similarity between the Cycle 3 basalts and Recent basalts. Trace element data indicate that the basanite of the Recent basalts has undergone some fractionation (mostly removal of olivine), but from a parental composition approaching that of the Cycle 3 basalt lava (Figs 23 and 24). Comparison with basalt lavas from the Upper Group of the caldera wall (Ablay *et al.*, 1995*b*) and the Teide–Pico Viejo stratovolcanic complex (Ablay *et al.*, 1995*b*, 1998) reveals no observable geochemical difference between intracaldera and extra-caldera basalts. There appears, therefore, not to have been any significant change in the composition of parental basaltic magmas spatially across the Las Cañadas volcano, or with time. Furthermore, the presence of long-lived extra-caldera regional fractures suggests that mafic magma has been intruded both laterally into the Las Cañadas volcano and from depth (Ablay & Martí, 1995). These fractures have acted as conduits for primitive mafic magmas, at least throughout Cycles 2 and 3 (Bryan *et al.*, 1998), and during the development of the Teide–Pico Viejo stratovolcanoes.

Petrological significance of nosean or haüyne

An unusual aspect of the petrological evolution of phonolitic explosive volcanism of the Las Cañadas edifice is

Table 4: Sulphur isotope data for nosean phenocryst separates from the Granadilla pumice

Sample number	Easting	Northing	Sample height (m)	Fall unit	Sample weight (mg)	S (wt %)	$\delta^{34}S$ nosean
111e	346·406	3111·71	1·17	1D	5·00	—	7·6
1i	349·39	3109·387	1·55	3	5·71	1·60	6·1
8k	347·76	3111·823	3·1	4	6·17	0·70	8·8
8o	347·76	3111·823	6·6	4	7·11	2·25	7·4

Sulphur isotope results in parts per thousand (per mil) relative to V-CDT. 2σ errors are $\pm 0{\cdot}2‰$. Analyses were performed using continuous flow isotope mass spectrometry (Glesemann *et al.*, 1994).

the apparent change from phenocrystic nepheline in the Ucanca Formation (1·56–1·07 Ma) to sulphur-rich nosean or haüyne in Cycles 2 and 3 (Bandas del Sur Formation), and the Guajara and Diego Hernández formations of the caldera wall (0·85–0·17 Ma; Martí *et al.*, 1994, 1997). Petrological data for the Bandas del Sur Formation are contradictory in terms of evidence for the magmas being sulphur-rich to account for crystallization of nosean–haüyne. Phonolitic pumice glass compositions indicate very low concentrations of dissolved sulphur (Fig. 22c). However, higher magmatic sulphur contents are indicated by the presence of sulphur-rich nosean–haüyne phenocrysts (Fig. 9b) and elevated SO_3 contents in apatites (Fig. 8a).

Isotopic studies of the sulphur-bearing minerals in the phonolites are used here to shed light on the origin of sulphur. $\delta^{34}S$ values for nosean crystal separates from the Granadilla pumice show a relatively restricted range from $+6{\cdot}1$ to $+8{\cdot}8‰$ (Table 4). The sulphate is distinctly heavier than sulphide gases analysed from active fumaroles on Teide, but compares well with sulphate emissions in underground water tunnels across Tenerife (Albert-Beltran *et al.*, 1990; Valentin *et al.*, 1990). The sulphur isotope data are comparable with isotopic determinations for other haüyne separates ($-1{\cdot}1$ to $+6{\cdot}6‰$) from Quaternary leucite-bearing volcanic rocks in Italy (Cavarretta & Lombardi, 1990), $\delta^{34}S$ values for anhydrite ($+9{\cdot}0$ to $+9{\cdot}2‰$) and glass ($+7{\cdot}8$ to $8{\cdot}4‰$) from the El Chichón eruption (Rye *et al.*, 1984), and whole pumices ($+7{\cdot}8$ to $+9{\cdot}0‰$) from the 1991 Pinatubo eruption (Imai *et al.*, 1993). Studies of the El Chichón and Pinatubo eruptions (e.g. Rye *et al.*, 1984; Pallister *et al.*, 1992, 1996; Hattori, 1993) have suggested a magmatic origin for sulphur. The euhedral character of nosean–haüyne phenocrysts in the Tenerife phonolites, and their inclusion in other silicate phases (mainly feldspar) indicate magmatic crystallization over the entrainment of xenocrysts.

The examination of several recent explosive eruptions has revealed that the mass of SO_2 released during the eruptions exceeded the amount originally dissolved in the erupted volume of silicate melt, requiring the existence of a separate SO_2-bearing gas phase (Wallace, 2001). Studies on the 1991 Pinatubo eruption indicate that an external source of sulphur was important in the crystallization of anhydrite and for the climatologically important SO_2 emissions (Pallister *et al.*, 1992, 1996; Hattori, 1993). As the solubility of sulphur as SO_4^{2-} is much higher than that of S^{2-} (Nagashima & Katsura, 1973; Carroll & Rutherford, 1987; Hattori, 1993), the progressive oxidation of the melt will not promote the crystallization of nosean or haüyne in the case of the phonolites. Oxygen fugacity estimates (Fig. 18) indicate that Tenerife magmas were not highly oxidized, and became slightly reduced with differentiation (see also Ablay *et al.*, 1998). Phonolitic glass compositions have variable, but low ($\leq 0{\cdot}1$ wt % as SO_3) sulphur contents, but significantly higher abundances are observed in the phonotephritic to tephriphonolitic glasses (Fig. 22c).

The lack of evidence for large amounts of dissolved sulphur requires the addition of sulphur from an external source for the phonolites. SO_2 discharged from mafic melts typically has $\delta^{34}S$ of $\sim +6{\cdot}0‰$ (Sakai *et al.*, 1984). Although the $\delta^{34}S$ value is dependent on temperature, fO_2 and fH_2O, degassing of SO_2 from underlying mafic melts provides an explanation for both the isotopic composition of nosean–haüyne phenocrysts (Table 4) and the elevated sulphur contents of apatites in the phonolites (Fig. 8a). The basaltic Dorsal Ridge system may also be an important source for mafic underplating of the Las Cañadas magmatic system to maintain an elevated abundance of sulphur (high fSO_2) in the phonolitic magma reservoir at shallow levels, and promoting nosean–haüyne crystallization over nepheline. The petrological and isotopic data thus indicate that the phonolite

magmas were probably associated with significant volumes of exsolved SO_2 gas, and potentially produced significant SO_2 emissions during the explosive eruptions.

CONCLUSIONS

The following aspects are considered important in describing the geochemistry of the Bandas del Sur Formation: (1) the bimodal nature of volcanic compositions; (2) the broad range of pumice glass compositions (phonotephrite–phonolite) in the pyroclastic deposits; (3) a diverse, 7–8-phase phenocryst assemblage for the phonolite pyroclastic deposits; (4) the geochemical continuity from parental basalts to phonolites, and the importance of fractional crystallization (involving the observed phenocryst assemblages) in developing the spectrum of compositions; (5) the petrological and geochemical differences between Cycles 2 and 3; (6) the apparent influence of contemporaneous basaltic volcanism of the adjacent Dorsal Ridge system on phonolitic explosive volcanism from the Las Cañadas volcano.

Trace element behaviour during crystal–liquid fractionation processes, from parental basaltic magmas to phonolites, can be grouped into the following: (1) those elements behaving incompatibly (e.g. K, Rb, Th, Nb, Zr, Hf, LREE); (2) elements that are strongly depleted, i.e. those behaving compatibly (e.g. Ti, Mg, Ca, P, Sr, Sc, Cr, Ni); (3) elements exhibiting later-stage compatibility during fractional crystallization [e.g. Na, Al, Ta, Ba, Sr, middle REE (MREE)]. Most elements showing late-stage compatibility reflect feldspar-dominated crystallization (e.g. Na, Al, Ba, Sr, Eu) or the appearance of titanite in the fractionating assemblage (e.g. Ta, MREE; Wolff, 1984).

The presence of reversely and normally zoned phenocrysts and bimodal to polymodal phenocryst compositions provides evidence that magma mixing has been an important process in the evolution of most of the phonolitic pyroclastic units. Mixing between phonolite and tephriphonolite magma characterizes some pyroclastic members of Cycle 2, and two distinct mixing events are recorded in several banded pumice-bearing ignimbrites of Cycle 3. The basaltic phenocryst assemblage in these banded pumice-bearing ignimbrites reflects a pre-eruptive mixing event between basaltic and intermediate (phonotephritic to mafic tephriphonolite) magmas. This periodic addition and mixing of basaltic magma may have ultimately triggered several eruptions. Long-term replenishment by basaltic magma of the chamber system and vapour transfer from underplated basaltic magma is interpreted to have elevated sulphur abundances in the evolved phonolitic magma reservoir.

The importance of AFC processes (Wolff & Palacz, 1989) is not supported by new geochemical data presented here. The non-zero intercepts on incompatible–incompatible element plots, indicative of AFC processes (Powell, 1984), cannot be duplicated when the full spectrum of magma compositions is plotted. Any Pb isotope variation (Wolff & Palacz, 1989) therefore needs to be reassessed in terms of other processes, especially magmatic recharge events considering the data presented here. Previously published geochemical data and 'co-magmatic relationships' also need to be reinterpreted with regard to an accurate stratigraphy.

ACKNOWLEDGEMENTS

We thank Giray Ablay, Sylvia Zafrilla, Chris Stephens, Tony Ewart and Ian Nicholls for valuable discussions on aspects of this manuscript. The XRF analyses were performed by Frank Audsley, and ICP-MS analyses by Donna Korke. The support and assistance provided by Ron Rasch and David Cousens during microprobe sessions are gratefully acknowledged. S.B. was supported by an APA scholarship. A small ARC grant to Ray Cas assisted with analytical costs. Field and technical support was provided by the Commission of the European Communities, DGXII, Environment Programme, Climatology and Natural Hazards Unit, in the framework of the contract EV5V-CT-0283, and by the DGICYT project PN-95-0002. Phil Kyle and Ian Ridley are thanked for supportive and constructive reviews of the manuscript.

REFERENCES

Ablay, G. J. (1997). Evolution of the Teide–Pico Viejo magmatic system (Tenerife, Canary Islands). Ph.D. thesis, University of Bristol, Bristol, 540 pp.

Ablay, G. J. & Martí, J. (1995). Stratigraphy and structure of the Teide–Pico Viejo complex. In: Martí, J. & Mitjavila, J. (eds) *A Field Guide to the Central Volcanic Complex of Tenerife (Canary Islands). Serie Casa de Los Volcanes No. 4*. Lanzarote: Cabildo Insular de Lanzarote, pp. 47–80.

Ablay, G. J., Ernst, G. G. J., Martí, J. & Sparks, R. S. J. (1995*a*). The ~2 ka subplinian eruption of Montaña Blanca, Tenerife. *Bulletin of Volcanology* **57**, 337–355.

Ablay, G. J., Mitjavila, J. M. & Wolff, J. A. (1995*b*). Petrology of precaldera and Teide–Pico Viejo volcanic rocks. In: Martí, J. & Mitjavila, J. M. (eds) *A Field Guide to the Central Volcanic Complex of Tenerife (Canary Islands). Serie Casa de Los Volcanes No. 4*. Lanzarote: Cabildo Insular de Lanzarote, pp. 81–90.

Ablay, G. J., Carroll, M. R., Palmer, M. R., Martí, J. & Sparks, R. S. J. (1998). Basanite–phonolite lineages of the Teide–Pico Viejo volcanic complex, Tenerife, Canary Islands. *Journal of Petrology* **39**, 905–936.

Albert-Beltran, J. F., Araña, V., Díez, J. L. & Valentín, A. (1990). Physical–chemical conditions of the Teide volcanic system (Tenerife, Canary Islands). *Journal of Volcanology and Geothermal Research* **43**, 321–332.

Ancochea, E., Fuster, J. M., Ibarrola, E., Cendrero, A., Coello, J., Hernan, F., Cantagrel, J. M. & Jamond, C. (1990). Volcanic evolution

of the island of Tenerife (Canary Islands) in the light of new K–Ar data. *Journal of Volcanology and Geothermal Research* **44**, 231–249.

Araña, V., Martí, J., Aparcio, A., García Cacho, L. & García, R. (1994). Magma mixing in alkaline magmas: an example from Tenerife, Canary Islands. *Lithos* **32**, 1–19.

Bacon, C. R. & Hirschmann, M. M. (1988). Mg/Mn partitioning as a test for equilibrium between coexisting Fe–Ti oxides. *American Mineralogist* **73**, 57–61.

Blake, S. & Campbell, I. H. (1986). The dynamics of magma-mixing during flow in volcanic conduits. *Contributions to Mineralogy and Petrology* **94**, 72–81.

Bohrson, W. A. & Clague, D. A. (1988). Origin of ultramafic xenoliths containing exsolved pyroxenes from Hualalai Volcano, Hawaii. *Contributions to Mineralogy and Petrology* **100**, 139–155.

Booth, B. (1973). The Granadilla Pumice deposit of southern Tenerife, Canary Islands. *Proceedings of the Geological Association* **84**, 353–370.

Brandle, J. L. (1973). Evolución geoquimica de los materiales volcánicos sálicos y alcalinos de la isla de Tenerife. *Estudios Geologicos* **29**, 5–51.

Bryan, S. E. (1998). Volcanology and petrology of the Granadilla Member, Tenerife (Canary Islands): constraints on the eruption dynamics, ignimbrite emplacement and caldera evolution. Ph.D. thesis, Monash University, Clayton, Vic., 632 pp.

Bryan, S. E., Martí, J. & Cas, R. A. F. (1998). Stratigraphy of the Bandas del Sur Formation: an extracaldera record of Quaternary phonolitic explosive eruptions from the Las Cañadas edifice, Tenerife (Canary Islands). *Geological Magazine* **135**, 605–636.

Bryan, S.E., Cas, R. A. F. & Martí, J. (2001). The 0·57 Ma plinian eruption of the Granadilla Member, Tenerife (Canary Islands): an example of complexity in eruption dynamics and evolution. *Journal of Volcanology and Geothermal Research* **103**, 209–238.

Carmichael, I. S. E. (1967). The iron–titanium oxides of salic volcanic rocks and their associated ferromagnesian silicates. *Contributions to Mineralogy and Petrology* **14**, 36–64.

Carroll, M. R. & Rutherford, M. J. (1987). The stability of igneous anhydrite: experimental results and implications for sulfur behaviour in the 1982 El Chichón trachyandesite and other evolved magmas. *Journal of Petrology* **28**, 781–801.

Cavaretta, G. & Lombardi, G. (1990). Origin of sulphur in the Quaternary perpotassic melts of Italy: evidence from haüyne sulphur isotope data. *Chemical Geology* **82**, 15–20.

Cox, K. G. (1983). The Karoo province of southern Africa: origin of trace element enrichment patterns. In: Hawkesworth, C. J. & Norry, M. J. (eds) *Continental Basalts and Mantle Xenoliths*. Nantwich, UK: Shiva, pp. 139–157.

Druitt, T. H., Mellors, R. A., Pyle, D. M. & Sparks, R. S. J. (1989). Explosive volcanism on Santorini, Greece. *Geological Magazine* **126**, 95–126.

Ewart, A. (1989). Eastern Australian petrology and geochemistry. In: Johnson, R. W. (ed.) *Intraplate Volcanism in Eastern Australia and New Zealand*. Sydney, N.S.W.: Cambridge University Press, pp. 189–248.

Fernández-Santin, S. & López, R. N. (1978). La extrusión fonolítico-traquítica de Montaña de Guaza, Tenerife (Canarias). *Estudios Geológicos* **34**, 375–387.

Fuster, J. M., Araña, V., Brandle, J. L., Navarro, M., Alonso, U. & Aparcio, A. (1968). *Geologia y Volcanologia de Las Islas Canarias: Tenerife*. Madrid: Instituto 'Lucas Mallada', CSIC, 218 pp.

Ghiorso, M. S. & Sack, R. O. (1991). Fe–Ti oxide geothermometry: thermodynamic formulation and the estimation of intensive variables in silicic magmas. *Contributions to Mineralogy and Petrology* **108**, 485–510.

Glesemann, A., Jäger, H.-J., Norman, A. L., Krouse, H. R. & Brand, W. A. (1994). On-line sulfur-isotope determination using an elemental analyser coupled to a mass spectrometer. *Analytical Chemistry* **66**, 2816–2819.

Hattori, K. (1993). High-sulfur magma, a product of fluid discharge from underlying mafic magma: evidence from Mount Pinatubo, Philippines. *Geology* **21**, 1083–1086.

Imai, A., Listanco, E. L. & Fujii, T. (1993). Petrologic and sulfur isotopic significance of highly oxidized and sulfur-rich magma of Mt. Pinatubo, Philippines. *Geology* **21**, 699–702.

Jurewicz, A. J. G. & Watson, E. B. (1988). Cations in olivine, part 1: Calcium partitioning and calcium–magnesium distribution between olivines and coexisting melts, with petrologic applications. *Contributions to Mineralogy and Petrology* **99**, 176–185.

Le Maitre, R. W. (ed.) (1989). A classification of igneous rocks and glossary of terms. *Recommendations of the International Union of Geological Sciences Subcommission on the Systematics of Igneous Rocks*. Oxford: Blackwell, 193 pp.

Lessing, P. & Grout, C. M. (1971). Haüynite from Edwards, New York. *American Mineralogist* **56**, 1096–1100.

Loucks, R. R. (1996). A precise olivine–augite Mg–Fe-exchange geothermometer. *Contributions to Mineralogy and Petrology* **125**, 140–150.

Luhr, J. F., Carmichael, I. S. E. & Varecamp, J. C. (1984). The 1982 eruptions of El Chichón volcano, Chiapas, Mexico: mineralogy and petrology of the anhydrite-bearing pumices. *Journal of Volcanology and Geothermal Research* **23**, 69–108.

Martí, J., Mitjavila, J. & Araña, V. (1994). Stratigraphy, structure and geochronology of the Las Cañadas caldera (Tenerife, Canary Islands). *Geological Magazine* **131**, 715–727.

Martí, J., Ablay, G. J., Bryan, S. & Mitjavila, J. (1995). Part II: description of field stops. In: Martí, J. & Mitjavila, J. (eds) *A Field Guide to the Central Volcanic Complex of Tenerife (Canary Islands). Serie Casa de Los Volcanes No. 4*. Lanzarote: Cabildo Insular de Lanzarote, pp. 93–156.

Martí, J., Hurlimann, M., Ablay, G. J. & Gudmundsson, A. (1997). Vertical and lateral collapses on Tenerife (Canary Islands) and other volcanic ocean islands. *Geology* **25**, 879–882.

Mitjavila, J. M. (1990). Aplicacio de tecniques de geoquimica isotopica i de geochronologia a l'estudi volcanologic de l'Edifici de Diego Hernández i la seva relacío amb la caldera de Las Cañadas (Tenerife). Ph.D. thesis, University of Barcelona, 258 pp.

Morimoto, M. (1988). Nomenclature of pyroxenes. *Mineralogical Magazine* **52**, 535–550.

Nagashima, S. & Katsura, T. (1973). The solubility of sulphur in Na_2O–SiO_2 melts under various oxygen partial pressures at 1100°C, 1250°C and 1300°C. *Chemical Society of Japan Bulletin* **46**, 3099–3103.

Neilsen, C. H. & Sigurdsson, H. (1981). Quantitative methods for electron microprobe analysis of sodium natural and synthetic glasses. *American Mineralogist* **66**, 547–552.

Norrish, K. & Hutton, J. T. (1969). An accurate X-ray spectrographic method for the analysis of a wide range of geological samples. *Geochimica et Cosmochimica Acta* **33**, 431–453.

Palacz, Z. A. & Wolff, J. A. (1989). Strontium, neodymium and lead isotope characteristics of the Granadilla pumice, Tenerife: a study of the causes of strontium isotope disequilibrium in felsic pyroclastic deposits. In: Saunders, A. D. & Norry, M. J. (eds) *Magmatism in the Ocean Basins. Geological Society, London, Special Publications* **42**, 147–159.

Pallister, J. S., Hoblitt, R. P. & Reyes, A. G. (1992). A basalt trigger for the 1991 eruptions of Pinatubo volcano? *Nature* **356**, 426–428.

Pallister, J. S., Hoblitt, R. P., Meeker, G. P., Knight, R. J. & Siems, D. F. (1996). Magma mixing at Mount Pinatubo: petrographic and chemical evidence from the 1991 deposits. In: Newhall, C. G. & Punongbayan, R. S. (eds) *Fire and Mud: Eruptions and Lahars of Mount Pinatubo, Philippines*. Seattle, WA: University of Washington Press, pp. 687–731.

Paradas Herrero, A. & Fernández Santín, S. (1984). Estudio vulcanologico y geoquimico del maar de la Caldera del Rey, Tenerife (Canarias). *Estudios Geológicos* **40**, 285–313.

Pearce, J. A., Alabaster, T., Shelton, A. W. & Searle, M. P. (1981). The Oman ophiolite as a Cretaceous arc–basin complex: evidence and implications. *Philosophical Transactions of the Royal Society of London, Series A* **300**, 299–317.

Powell, R. (1984). Inversion of the assimilation and fractional crystallization (AFC) equations; characterization of contaminants from isotope and trace element relationships in volcanic suites. *Journal of the Geological Society, London* **141**, 447–452.

Ridley, W. I. (1970). The petrology of the Las Cañadas volcanoes, Tenerife, Canary Islands. *Contributions to Mineralogy and Petrology* **26**, 124–160.

Robinson, P., Spear, F. S., Schumacher, J. C., Laird, J., Klein, C., Evans, B. W. & Doolan, B. L. (1981). Phase relations of metamorphic amphiboles: natural occurrence and theory. In: Veblen, D. R. & Ribbe, P. H. (eds) *Amphiboles: Petrology and Experimental Phase Relations. Mineralogical Society of America, Reviews in Mineralogy* **9B**, 1–228.

Roeder, P. L., Campbell, I. H. & Jamieson, H. E. (1979). A re-evaluation of the olivine–spinel geothermometer. *Contributions to Mineralogy and Petrology* **68**, 325–334.

Rutherford, M. J. (1993). Experimental petrology applied to volcanic processes. *EOS Transactions, American Geophysical Union* **74**, 49, 55.

Rutherford, M. J. & Hill, P. M. (1993). Magma ascent rates from amphibole breakdown: an experimental study applied to the 1980–1986 Mount St. Helens eruptions. *Journal of Geophysical Research* **98**, 19667–19685.

Rye, R. O., Luhr, J. F. & Wasserman, M. D. (1984). Sulfur and oxygen isotopic systematics of the 1982 eruptions of El Chichón volcano, Chiapas, Mexico. *Journal of Volcanology and Geothermal Research* **12**, 109–123.

Sakai, H., Des Marais, D. J., Ueda, A. & Moore, J. G. (1984). Concentrations and isotope ratios of carbon, nitrogen and sulfur in ocean-floor basalts. *Geochimica et Cosmochimica Acta* **48**, 2433–2441.

Schmincke, H.-U. & Swanson, D. A. (1967). Ignimbrite origin of eutaxites from Tenerife. *Neues Jahrbuch für Geologie und Palaeontologie, Monatshefte* **11**, 700–703.

Scott, P. W. (1976). Crystallization trends of pyroxenes from the alkaline volcanic rocks of Tenerife, Canary Islands. *Mineralogical Magazine* **40**, 805–816.

Shotton, F. W. & Williams, R. E. G. (1971). Birmingham University radiocarbon dates V. *Radiocarbon*, **13**(2), 150.

Stolz, A. J. (1985). The role of fractional crystallization in the evolution of the Nandewar volcano, north-eastern New South Wales, Australia. *Journal of Petrology* **26**, 1002–1026.

Sun, S.-S. & McDonough, W. F. (1989). Chemical and isotopic systematics of oceanic basalts. In: Saunders, A. D. & Norry, M. J. (eds) *Magmatism in the Ocean Basins. Geological Society, London, Special Publications* **42**, 313–345.

Valentin, A., Albert-Beltran, J. F. & Diez, J. L. (1990). Geochemical and geothermal constraints on magma bodies associated with historic activity, Tenerife (Canary Islands). *Journal of Volcanology and Geothermal Research* **44**, 251–264.

Wallace, P. J. (2001). Volcanic SO_2 emissions and the abundance and distribution of exsolved gas in magma bodies. *Journal of Volcanology and Geothermal Research* **108**, 85–106.

Wolff, J. A. (1983). Petrology of Quaternary pyroclastic deposits from Tenerife, Canary Islands. Ph.D. thesis, University of London, 542 pp.

Wolff, J. A. (1984). Variation in Nb/Ta during differentiation of phonolitic magma, Tenerife, Canary Islands. *Geochimica et Cosmochimica Acta* **48**, 1345–1348.

Wolff, J. A. (1985). Zonation, mixing and eruption of silica-undersaturated alkaline magma: a case study from Tenerife, Canary Islands. *Geological Magazine* **122**, 623–640.

Wolff, J. A. & Palacz, Z. A. (1989). Pb isotope and trace-element variation in the phonolitic Granadilla Series, Tenerife: evidence for recycling within an ocean island volcano. *Mineralogical Magazine* **53**, 519–525.

Wolff, J. A. & Storey, M. (1983). The volatile component of some pumice-forming alkaline magmas from the Azores and Canary Islands. *Contributions to Mineralogy and Petrology* **82**, 66–74.

Wolff, J. A. & Storey, M. (1984). Zoning in highly alkaline magma bodies. *Geological Magazine* **121**, 563–575.

Yanagisawa, F. & Sakai, H. (1983). Thermal decomposition of barium sulfate–vanadium pentaoxide–silica glass mixtures for preparation of sulfur dioxide in sulfur isotope ratio measurements. *Analytical Chemistry* **55**, 985–987.

APPENDIX A

Table A1: Major and trace element abundances for pyroclastic and lava members of the Bandas del Sur Formation

Sample:	59	76	119	134	18E	130	85	43	120MS
Map unit:	Lower Group	Cycle 3 basalts	Cycle 3 basalts	Recent basalts	Unit E	Arico	Saltadero	El Rio	Abades
Lithology:	lava	lava	lava	lava	pumice fall	ignimbrite	ignimbrite	pumice fall	ignimbrite
X:	356·632	349·55	354·796	353·919	351·889	359·994	349·63	353·029	357·737
Y:	3110·91	3104·98	3112·033	3108·497	3113·828	3114·753	3103·553	3109·84	3112·154
Major elements (wt %)									
SiO_2	59·28	42·43	47·34	43·03	62·82	60·98	61·05	61·35	56·2
TiO_2	1·15	3·19	3·26	3·59	0·84	0·93	0·82	0·61	1·64
Al_2O_3	19·38	10·71	16·75	12·72	20·47	18·38	18·54	18·06	19·07
Fe_2O_3T	3·83	14·41	11·45	14·07	3·84	3·55	3·39	3	5·82
MnO	0·21	0·18	0·21	0·19	0·21	0·22	0·23	0·22	0·2
MgO	0·96	13·92	3·98	9·62	1·01	0·99	0·68	2·03	1·91
CaO	2·06	10·27	8·89	10·62	0·81	1·07	0·97	2·37	3·99
Na_2O	8·37	2·93	4·83	4·45	4·73	8·42	9·08	6·71	6·99
K_2O	4·55	1·16	1·95	0·82	5·21	5·32	5·1	5·57	3·78
P_2O_5	0·2	0·66	1·34	0·91	0·07	0·13	0·14	0·09	0·4
LOI	0·88	0·19	0·78	−0·18	10·39	4·96	4·19	9·07	2·64
Trace elements (ppm)									
Ba	1289	348	730	424	125	787	360	84	1345
Rb	111	26	47	29	134	99	106	139	98
Sr	647	726	1283	916	32	60	12	37	835
Y	44	25	40	32	55	42	48	54	45
Zr	866	227	464	327	892	739	815	998	643
Nb	219	66	119	81	229	198	227	244	192
Th	24	3	13	4	17	19	23	18	13
U	6	1	1	1	4	4	5	5	3
Pb	10	2	5	3	15	9	10	11	11
Ga	—	24	—	27	40	—	—	37	38
Zn	127	117	121	124	85	134	145	90	101
Cu	b.d.	75	17	64	6	b.d.	b.d.	4	12

Sample:	59	76	119	134	18E	130	85	43	120MS
Map unit:	Lower Group	Cycle 3 basalts	Cycle 3 basalts	Recent basalts	Unit E	Arico	Saltadero	El Rio	Abades
Lithology:	lava	lava	lava	lava	pumice fall	ignimbrite	ignimbrite	pumice fall	ignimbrite
X:	356·632	349·55	354·796	353·919	351·889	359·994	349·63	353·029	357·737
Y:	3110·91	3104·98	3112·033	3108·497	3113·828	3114·753	3103·553	3109·84	3112·154
Ni	b.d.	333	6	168	7	b.d.	b.d.	5	10
V	39	264	188	284	42	33	36	34	90
Cr	4	695	6	291	7	6	6	3	18
Hf	—	5	—	6	14	—	—	15	11
Cs	—	0	—	0	2	—	—	2	1
Sc	2	28	7	28	10	b.d.	b.d.	15	13
Ta	—	4	—	5	12	—	—	12	11
Co	19	75	29	59	7	9	9	8	13
Ge	—	3	—	3	3	—	—	3	3
La	183	40	119	52	126	170	188	115	109
Ce	259	88	192	110	219	249	287	206	216
Pr	—	10	—	13	24	—	—	20	22
Nd	91	44	79	54	84	82	94	68	81
Sm	—	8	—	10	13	—	—	10	13
Eu	—	3	—	3	3	—	—	2	4
Gd	—	6	—	8	10	—	—	8	10
Tb	—	1	—	1	2	—	—	1	1
Dy	—	5	—	7	9	—	—	8	8
Ho	—	1	—	1	2	—	—	2	2
Er	—	2	—	3	5	—	—	5	4
Tm	—	0	—	0	1	—	—	1	1
Yb	—	2	—	2	4	—	—	4	3
Lu	—	0	—	0	1	—	—	1	0

Table A1: continued

Sample:	Unit 1 ($n = 5$)	Unit 3 ($n = 4$)	Unit 4 ($n = 7$)	Unit 5 ($n = 5$)	41	93LM	93LMb	36	93A
Map unit:	Granadilla	Granadilla	Granadilla	Granadilla	Poris	La Mareta	La Mareta	Wavy	El Abrigo
Lithology:	pumice fall	pumice fall	pumice fall	ignimbrite	ignimbrite	ignimbrite	pumice clast	pumice fall	ignimbrite
X:	346·406	349·39	347·76	350·874	359·949	346·316	346·316	360·176	346·316
Y:	3111·71	3109·387	3111·823	3112·688	3115·402	3101·023	3101·023	3115·778	3101·023
Major elements (wt %)									
SiO_2	61·1	61	61·17	61·15	58·73	57·73	56·98	56·9	58·63
TiO_2	0·57	0·51	0·54	0·69	0·69	0·48	1·39	0·58	1·06
Al_2O_3	19·66	19·98	19·73	19·46	19·89	20·56	19·28	19·16	18·92
Fe_2O_3T	3·37	3·43	3·35	3·35	3·71	2·8	4·65	2·86	4·23
MnO	0·25	0·27	0·25	0·21	0·19	0·18	0·15	0·14	0·21
MgO	0·64	0·56	0·7	0·72	1·77	0·38	1·22	1·9	1·46
CaO	0·82	0·72	0·72	1·26	1·22	2·2	3·51	2·75	2·95
Na_2O	7·52	7·51	6·83	7·26	7·17	9·44	7·55	9·35	7·14
K_2O	6·01	5·98	6·67	5·82	6·49	6·18	4·94	6·24	5·22
P_2O_5	0·06	0·04	0·04	0·06	0·15	0·05	0·32	0·13	0·19
LOI	7·22	8·26	7·55	11·62	15·73	5·19	1·47	8·43	10·39
Trace elements (ppm)									
Ba	252	81	52	175	168	63	1300	242	360
Rb	191	207	194	171	214	206	117	160	140
Sr	42	24	16	137	169	60	517	125	201
Y	51	51	50	45	29	26	39	16	44
Zr	1346	1508	1348	1073	1435	1447	689	971	1075
Nb	299	322	301	264	236	230	175	136	238
Th	42	47	42	33	48	46	18	34	30
U	10	11	10	6	3	10	7	7	6
Pb	17	19	17	14	18	17	9	15	12
Ga	—	—	—	—	—	—	—	—	—
Zn	173	187	173	147	154	126	99	100	139
Cu	b.d.	b.d.	b.d.	b.d.	7	b.d.	b.d.	12	b.d.

Sample:	Unit 1 (n = 5)	Unit 3 (n = 4)	Unit 4 (n = 7)	Unit 5 (n = 5)	41	93LM	93LMb	36	93A
Map unit:	Granadilla	Granadilla	Granadilla	Granadilla	Poris	La Mareta	La Mareta	Wavy	El Abrigo
Lithology:	pumice fall	pumice fall	pumice fall	ignimbrite	ignimbrite	ignimbrite	pumice clast	pumice fall	ignimbrite
X:	346·406	349·39	347·76	350·874	359·949	346·316	346·316	360·176	346·316
Y:	3111·71	3109·387	3111·823	3112·688	3115·402	3101·023	3101·023	3115·778	3101·023
Ni	b.d.	6	b.d.	b.d.	b.d.	b.d.	b.d.	11	6
V	35	33	34	23	42	29	79	32	70
Cr	7	8	7	5	13	5	6	10	17
Hf	—	—	—	—	—	—	—	—	—
Cs	—	—	—	—	—	—	—	—	—
Sc	b.d.	b.d.	b.d.	b.d.	b.d.	b.d.	3	1	b.d.
Ta	—	—	—	—	—	—	—	—	—
Co	13	15	12	6	4	11	15	14	9
Ge	—	—	—	—	—	—	—	—	—
La	201	214	207	201	141	126	110	81	166
Ce	264	272	268	270	184	170	209	108	248
Pr	—	—	—	—	—	—	—	—	—
Nd	66	64	68	75	41	28	69	22	69
Sm	—	—	—	—	—	—	—	—	—
Eu	—	—	—	—	—	—	—	—	—
Gd	—	—	—	—	—	—	—	—	—
Tb	—	—	—	—	—	—	—	—	—
Dy	—	—	—	—	—	—	—	—	—
Ho	—	—	—	—	—	—	—	—	—
Er	—	—	—	—	—	—	—	—	—
Tm	—	—	—	—	—	—	—	—	—
Yb	—	—	—	—	—	—	—	—	—
Lu	—	—	—	—	—	—	—	—	—

X, Y are UTM grid coordinates (Zone 28, northern hemisphere) for sample localities. Major elements normalized to 100%, loss on ignition (LOI) free, with all Fe as Fe_2O_3. Samples with complete trace element data were analysed by inductively coupled plasma-mass spectrometry (ICP-MS) at Monash University; others by XRF with trace element abundances LOI-free normalized. b.d., below detection limit; *n*, number of samples. XRF analyses were performed on a Philips PW1400 spectrometer at the University of Queensland. Major elements were fused on glass discs and trace elements on pressed powder pellets. The complete dataset can be downloaded from the *Journal of Petrology* website at http://www.petrology.oupjournals.org.

APPENDIX B: ANALYTICAL TECHNIQUES AND METHODS

X-ray fluorescence

Pumice samples were lightly crushed using only a tungsten carbide concentric ring (tema) mill where the clast size was small enough, or a primary jaw crusher to first reduce clast size. Two-stage crushing (jaw crushing followed by tungsten carbide tema mill) was required for whole-rock samples. Lithic fragments and the outer parts of samples that were altered (e.g. groundwater cement) were removed before milling, and any remaining contaminating lithic fragments were also removed before tema milling. Some ash loss, especially for pumice samples, was unavoidable during both crushing stages.

Major and trace element concentrations determined at the Department of Earth Sciences, University of Queensland, by X-ray fluorescence spectrometry (XRF) used a Philips PW1400 wavelength-dispersive X-ray spectrometer, with Philips PW1730 60 kV X-ray generator, Philips PW1500 72 position sample changer, and Rh and Au anode X-ray tubes. Fused discs for major element analysis were prepared by the Norrish & Hutton (1969) method. Pressed pellets (trace element analysis) prepared at University of Queensland used an in-house technique similar to those used at the Department of Geochemistry, University of Capetown. All major element XRF data have been normalized to 100% on an anhydrous basis, and trace element data have been normalized on a volatile loss on ignition (LOI)-free basis. LOI was determined by weight loss after drying sample powders in an oven. Approximately 1–1·5 g of sample in a preweighed ceramic crucible was heated overnight at 105°C and reweighed. The samples were then heated to 800°C for 2–3 h, then reweighed when cool. At higher temperatures, the phonolite powders fused, rendering the ceramic crucibles unusable. Fused discs were prepared from the ignited powders.

Inductively coupled plasma-mass spectrometry (ICP-MS)

Selected samples were analysed for trace and rare earth elements by inductively coupled plasma-mass spectrometry (ICP-MS) at the Department of Earth Sciences, Monash University. Powders were prepared using an agate concentric ring mill.

Chemistry

Aliquots (100 mg) of each sample were digested for 24–48 h in Savillex-type Teflon bombs at 150°C in a mixture of distilled HF (3 ml) and HNO_3 (1 ml). Sample solutions were taken to dryness in HEPA-filtered clean air cabinets, followed by conversion of fluorides to nitrates with two additions of concentrated HNO_3. Samples were then taken into solution with 50 g of 2·5% HNO_3 (made up with sub-boiled distilled concentrated HNO_3 and 18·2 Mohm Millipore water). All samples were also made up to 100 ppb indium to serve as an internal standard to correct for instrument drift. One analytical blank and at least three standard solutions (based on 1:50 dilutions of 50 mg, 100 mg and 150 mg of digested US Geological Survey rock standard BHVO-1) were typically prepared with each batch of samples. The STM-1 syenite standard was also used as a more appropriate standard with similar trace and rare earth element concentrations to the Tenerife phonolites. Total dilution factors were calculated by weight for each sample and standard. US Geological Survey rock standards BHVO-1 and AGV-1 (and STM-1) served as check standards to monitor accuracy during the analysis procedure.

Mass spectrometry

Diluted rock solutions were analysed by inductively coupled plasma mass spectrometry (ICP-MS) using a VG PlasmaQuad PQ2+ in peak jumping mode with the electron multiplier operating in pulse-counting mode for maximum sensitivity and analytical precision. One or two isotopes were chosen for each element of interest based on considerations of isobaric interferences. Five blocks of data were obtained for each sample, with each block comprising 50 sweeps through the mass spectrum using three points per mass and five DAC steps per point. Instrumental drift corrections were accomplished using a combination of the In internal standard as well as repeat analyses of BHVO-1 (or STM-1 every five samples), permitting serial drift corrections on an element-by-element basis using an in-house data reduction computer program. Total analytical blanks (comprising both chemistry and mass spectrometer components) were typically <20 ppb for all elements, making blank corrections <2% for most geological samples and usually <0·1%.

Estimate of precision and accuracy

Precision (in-run statistics quoted as two standard errors of the mean) was typically better than 5% for each element. Determination of analytical accuracy was based on multiple analyses of US Geological Survey rock standards BHVO-1, AGV-1 and STM-1, and was typically better than 10% for most elements at the 95% confidence level. Exceptions include Gd, Dy and Er, which have LREE oxide interferences, and Tb, Ho, Tm and Lu, which typically occur at very low concentrations.

Electron microprobe analysis

Sixty polished and carbon-coated thin sections were analysed by electron microprobe to determine mineral

and glass chemistry. Analysis was undertaken at the Centre for Microscopy & Microanalysis, University of Queensland, using a JEOL 8800-L (wavelength-dispersive) electron microprobe. Analyses were performed with an accelerating voltage of 15 kV and with a probe current of 15 nA. Data were corrected on-line using the ZAF correction procedure. All phases were analysed with a 1 μm probe diameter, except for feldspars, aegirine, biotite, kaersutite and glass, which were analysed using a probe diameter of 10 μm to avoid volatilization of alkali elements. During glass analyses, the stage was moved slowly and continuously to also reduce the effects of alkali migration from the probe target volume (Neilsen & Sigurdsson, 1981). Precision and accuracy for each analytical run were checked by comparing results of a suite of geological and oxide standards of known composition, analysed at the start and end of each analytical run.

Stable isotope analysis

Crystal and glass separates were prepared from lightly crushed pumice clasts using a tungsten carbide concentric ring mill. The crushed sample was sieved using 14 mesh (1·4 mm diameter) and 100 mesh (50 μm) sieves. The >100 mesh fraction was used for mineral and glass separates, and was washed to remove any fine glass, and dried. Minerals were separated from glass by heavy liquid methods. Feldspar, biotite, nosean and glass were then hand picked from the heavy liquid separates, and composite grains or grains with inclusions were avoided.

Sulphur isotope ratios were measured at two laboratories, at the University of Queensland and the University of Karlsruhe. At the University of Queensland, the nosean sample was mixed with V_2O_5 and SiO_2 and then thermally decomposed to extract SO_2 by heating from 600 to 900°C (Yanagisawa & Sakai, 1983). Isotopic analyses of extracted sulphur dioxide were performed with an MM602E mass spectrometer using NBS 122 [0·5‰ Canyon Diablo Troilite (CDT)] and NBS 123 (17·0‰ CDT) to establish a calibration curve. All isotopic data are reported in per mil relative to CDT with analytical uncertainties better than $\pm 0{\cdot}3$‰ CDT (1σ) for homogeneous mineral separates. M. Loesson performed the analyses at the Institute for Petrography and Geochemistry, University of Karlsruhe, using continuous flow isotope mass spectrometry (Glesemann *et al.*, 1994). These values are reported as per mil deviation relative to Vienna-Canyon Diablo Troilite (V-CDT). The standard used in the analysis is a silver sulphide (IAEA-S-1), with $\delta^{34}S = -0{\cdot}3$‰. Analytical uncertainty is $\pm 0{\cdot}1$‰ (1σ).